Structural insights into the recruitment of viral Type 2 IRES to ribosomal preinitiation complex for protein synthesis

Deepakash Das and Tanweer Hussain

Department of Developmental Biology and Genetics, Indian Institute of Science, Bengaluru, INDIA. PIN-560012

*Correspondence: hussain@iisc.ac.in

Abstract

Picornaviruses employ internal ribosome entry sites (IRESs) in their genomic RNA to hijack the host's translational machinery. The picornavirus, Encephalomyocarditis virus, employs a type 2 IRES present in its 5'UTR and requires 43S ribosomal preinitiation complex (PIC), the central domain of eukaryotic initiation factor (eIF) 4G, eIF4A, and an essential ITAF (IRES trans-acting factor)-polypyrimidine tract binding protein 1 (PTB1) to form 48S PIC. In this study, we have used cryo-electron microscopy (cryo-EM) to determine the structure of EMCV IRES-bound mammalian 48S PIC in a scanning-arrested closed state at the start codon. The EMCV IRES domains contacts initiator tRNA ($tRNA_i$) and 40S head at the inter-subunit interface, which reveals an altogether unique mechanism used by viruses to capture host translational machinery for its protein synthesis. The $tRNA_i$ is held away from the 40S body in contrast to canonical cap-dependent translation while the domain I apical region of EMCV IRES mimics 28S rRNA of 60S to interact with 40S ribosomal head proteins- uS13 and uS19. The structural analysis account for numerous biochemical studies on Type 2 IRES and shows how Type 2 IRES interacts with 43S PIC to form 48S PIC. This study provides mechanistic insights for understanding EMCV IRES-mediated translation initiation, which could be extrapolated to other IRESs sharing similar motifs and factor requirements including type 1 viral IRESs.

42 **Introduction:**

43

44 Eukaryotic translation initiation occurs in two different modes- Cap-dependent and Cap-
45 independent. Cap-dependent translation initiation in eukaryotes can be divided into four
46 major steps- (i) formation of 43S ribosomal PIC [40S subunit in complex with eIF1, eIF1A, eIF3,
47 eIF5 and ternary complex (eIF2-GTP-tRNA$_i$)]; (ii) recruitment of 43S PIC to 5'end of capped
48 mRNA, mediated by eIF4F complex (formed by eIF4E,eIF4G and eIF4A) yielding 48S complex
49 (48S PIC); (iii) scanning of 5' untranslated region (UTR) of mRNA and start codon recognition;
50 and (iv) joining of large 60S ribosomal subunit to form elongation-competent 80S ribosomal
51 complex. Among these, major rate-limiting steps include- the regulation of available tRNA$_i$ as
52 the ternary complex (eIF2.GTP.Met-tRNA$_i$) and recruitment of mRNA on 43S PIC (*Jackson et*
53 *al 2010; Brito Querido et al 2024*). Cryo-EM studies on eukaryotic canonical 48S PICs from
54 yeast (*Hussain et al 2014; Llacer et al 2015*) to humans (*Eliseev et al 2018; Simonetti et al*
55 *2020; Brito Querido et al 2020; Yi et al 2022; Brito Querido et al 2024; Petrychenko et al 2024*)
56 have revealed various interactions among the initiation factors, mRNA, and ribosome in
57 scanning (P_{OUT} or open) state and scanning-arrested (P_{IN} or closed) states. In mammals, 48S
58 PIC formation is mediated by the interaction of eIF3 and eIF4G (*Villa et al 2013*) and recent
59 attempts to understand the mammalian canonical 48S PIC could capture interactions of eIF4
60 proteins (eIF4G and eIF4A) with eIF3 (*Brito Querido et al 2020; Brito Querido et al 2024*).

61

62 Alternatively, several positive strand RNA viruses use Internal Ribosome Entry Sites (IRESs),
63 which are internal cis-acting sequences present in 5' UTR of mRNA that drive the assembly of
64 translation initiation complex without the requirement of 7-methylguanosine cap (*Martínez-*
65 *Salas et al 2018*), initially reported in picornaviruses such as poliovirus (PV) and
66 encephalomyocarditis virus (EMCV) RNA genome (*Jang et al 1988; Pelletier and Sonenberg,*
67 *1988; Trono et al 1988*). As of 2020, the IRESbase database reported 1328 IRESs, out of which
68 554 were viral IRESs from 198 viruses (*Zhao et al 2020*). These RNA elements have unique
69 secondary and tertiary structures, which allows them to hijack the host translational
70 machinery and promote translation initiation internally by recruitment of host ribosome,
71 canonical eIFs, and IRES trans acting factors (ITAFs) via multiple RNA–RNA and RNA–protein
72 interactions (*Lee et al 2017; Martinez-Salas et al 2018*). The IRESs lack sequence homology
73 and enfolds different structural organization, thus requiring different eIFs for the assembly of

74 48S PICs (*Jackson et al 2010*). The type 1 IRES (represented by PV) and type 2 IRES (EMCV)
75 requires almost all eIFs, except eIF4E or N terminal of eIF4G for the formation of 48S PIC
76 (*Lozano and Martinez-Salas, 2015)*. However, initiation on the latter does not require
77 scanning for start codon recognition (*Kaminski et al 1994; Sweeney et al 2014)*. The type 3
78 IRES (Hepatitis C virus- HCV) does not require eIF4 factors or scanning for 48S PIC formation
79 (*Niepmann and Gerresheim 2020*). The type 4 IRES (Cricket paralysis virus- CrPV intergenic
80 IRES) initiates without the requirement of any eIFs and $tRNA_i$ (*Johnson et al 2017*). The HCV
81 IRES and CrPV intergenic IRES directly interacts with host 40S ribosome, however they differ
82 in their mechanism of attachment. Where, the CrPV IRES (type 4) mimics anticodon-codon
83 interaction via pseudoknot 1 to bind with ribosome in an elongation-competent state (*Petrov*
84 *et al 2016; Fernandez et al 2014*) the HCV IRES (type 3) binds to the solvent side of 40S subunit
85 by replacing eIF3 and directly interacts with expansion segment (ES7) of 18S rRNA and
86 ribosomal proteins near mRNA exit channel, thus placing the initiation codon at the P-site
87 (*Hashem et al 2013; Niepmann and Gerresheim 2020; Brown et al 2022*). While the structures
88 of ribosome-bound type 4 (*Spahn et al 2004; Fernandez et al 2014; Muhs et al 2015; Murray*
89 *et al 2016; Pisareva et al 2018; Acosta-Reyes et al 2019; Abaena et al 2020*) and type 3 IRES
90 (*Spahn et al 2004; Boehringer et al 2005; Hashem et al 2013; Yamamoto et al 2014; Quade et*
91 *al 2015; Yamamoto et al 2015; Yokoyama et al 2019; Brown et al 2022*) have been determined,
92 there is no structural information about Type 2 and Type 1 IRES and their mode of recruitment
93 to 48S PIC.
94
95 The 5'UTR of EMCV, genera Cardiovirus and Picornaviridae family (*International Committee*
96 *on Taxonomy of Viruses Executive Committee, 2020*) folds into various stem-loops numbered
97 D-L, where domains H-L, followed by the initiation codon at the 834th residue (~450
98 nucleotides in length) make a functional IRES moiety (*Carocci et al 2012*). It requires the core
99 of 43S PIC, the central domain of eIF4G, eIF4A, and an essential ITAF-polypyrimidine tract
100 binding protein 1 (PTB1), and the presence of eIF4B enhances 48S formation (*Hellen and*
101 *Wimmer 1995; Martinez-Salaz et al 2018; Sweeney et al 2014*). Functional characterization of
102 these domains showed H, and I interact with 40S ribosomal subunit (*Chamond et al 2014*),
103 and domain J-K recruits eIF4G, enhanced by eIF4A (*Pestova et al 1996; Lomakin et al 2000*).
104 The structure of domain J-K-eIF4G1(HEAT1)-eIF4A revealed that positively charged patches
105 on the eIF4G1-HEAT1 domain interact with two separated negatively charged clefts (in

domains J and St) without perturbing its innate function of recruiting eIF4A (*Imai et al 2016; Imai et al 2023*). The binding sites for PTB1 were revealed to be dispersed, encompassing domains H to L (*Kafasla et al 2009*). These domains function as a single entity to form 48S PIC and any mutation in conserved IRES motifs can drastically affect the translation rates (*Fernández-Miragall et al 2009; Fernández et al 2011*). For example, the RAAA and GNRA loop in the domain I of type 2 IRES are crucial for IRES activity (*Robertson et al 1999*), and the GNRA loop is also found in other IRES families such as type 1 (poliovirus) and type 5 (Aichi virus A) picornaviruses (*Abdullah et al 2023*). The inherent flexibility within the IRES domains provides a challenge for structural studies of full-length IRES and to capture IRES in the context of 48S PIC. EMCV IRES can independently interact with 40S subunit without any eIFs (*Chamond et al 2014*) and does not require scanning to recognize the start codon (*Pestova et al 1996*), unlike type 1 IRESs, which scan for the start codon (*Sweeney et al 2014*). Besides, EMCV IRES can form 48S PIC with HEAT1-eIF4G without the requirement of eIF4G residues 1015-1104 that are known to interact with eIF3 (*Lomakin et al 2000*). These residues are indispensable in case of canonical initiation on capped mRNAs and for type 1 IRESs (*Villa et al 2013; Sweeney et al 2014*). However, how EMCV IRES interacts with 40S subunit, or what molecular interactions are essential to form the EMCV IRES-48S PIC remains a question.

In this study, we have used pull-down assay to isolate EMCV IRES-bound 48S PIC from Rabbit Reticulocyte Lysate (RRL) and subjected the complex to cryo-electron microscopy (cryo-EM) analysis. The cryo-EM map of EMCV IRES-bound 48S PIC, henceforth mentioned as EMCV IRES-48S PIC, shows densities corresponding to EMCV IRES domains that reveal how EMCV IRES contacts the ternary complex and 40S head at the inter-subunit interface. The structural details presented here account for numerous biochemical studies that have been reported earlier on Type 2 IRES. Furthermore, the structural analysis suggests how Type 2 IRES would interact with 43S PIC to form 48S PIC. Importantly, the study reveals a unique strategy used by viral IRES to capture the host translational apparatus for making viral polypeptide.

138 **Results:**

139

140 1. Overview and features of EMCV IRES-48S PIC

141

142 To isolate 48S PIC on EMCV IRES, we used a Talon affinity-based pull-down from nuclease-
143 treated RRL. EMCV IRES RNA used harboured residues from 280 to 905 with AUG (start codon)
144 at 834th position. PTB1 was recombinantly overexpressed with an N-terminal 6X His tag,
145 followed by a 3C protease cleavage site. PTB1 was incubated with the IRES, followed by RRL
146 addition, and 48S PIC was stalled using GMP-PnP. The complex was eluted from the Talon
147 matrix employing 3C protease cleavage and pelleted (Sup. Fig. 1.1 A). The EMCV IRES-48S PIC
148 was subsequently analysed by Cryo-EM. The processed data yielded 3 major classes- (i) 40S
149 without any factors- Map A, (ii) 40S-IRES-tRNA$_i$- Map B, and (iii) 40S-IRES-ternary complex-
150 Map B1, namely, EMCV IRES-48S PIC (Sup. Fig. 1.1 B). Map B and Map B1 have an overall
151 resolution of 4.6 Å and 5.0 Å, respectively (Sup. Fig. 1.1 B). The core of 40S is at around 4.0 Å,
152 and the local resolution across the maps was largely in the range of 4.0-8 Å (Sup. Figs. 1.2 A
153 and B). Only the extreme tip of beak of 40S in Map B1 (Sup. Fig. 1.2 A) and ends of IRES and
154 eIF2γ are around 12 Å in Map B2 (Sup. Figs 1.2 B).

155

156 The cryo-EM densities in EMCV IRES-48S PIC correspond to 40S, tRNA$_i$, eIF2α, eIF2γ, and RNA
157 in the mRNA channel, along with an extra density connecting 40S ribosomal head to tRNA$_i$
158 (Fig. 1 A-B). However, it lacks distinct density for PTB1, eIF4G, eIF4A, and eIF3, and hence
159 these factors are not modelled. Since nuclease-treated RRL lacked endogenous RNA, the
160 presence of density for mRNA in the channel indicates trapping of EMCV IRES in 48S PIC. Also,
161 the density connecting 40S head to tRNA$_i$ in Map B and B1 could be assigned to a double-
162 stranded RNA structure found in EMCV IRES (Fig. 1 A-B).

163

164 Besides, an extra density is evident at the mRNA entry site, contacting 40S ribosomal proteins-
165 uS3, eS10, and uS5 and h16 (Helix 16) of 18S rRNA (Sup. Fig. 1.2 C). In the human 48S PIC, this
166 region positions eIF3g-RRM (RNA recognition motif) and downstream ORF (Sup. Fig.1.2 D)
167 (*Brito Querido et al 2020; Brito Querido et al 2024)*. We anticipate that this extra density in
168 EMCV IRES-48S PIC could be contributed by downstream ORF; however, it's difficult to assign
169 it to eIF3g-RRM due to the lack of eIF3 (core/peripheral) density. Furthermore, our recent

170 study on interaction of yeast eIF4B with 40S ribosome suggested occupancy of eIF4B (N
171 terminal-RRM) in the same region (*Datey et al 2025*), which opens up the possibility of
172 mammalian eIF4B-NT-RRM to bind to this region in the absence of eIF3, although in the
173 human 48S PIC eIF4B was tentatively positioned slightly away from this location (*Brito Querido*
174 *et al 2024)*. An interesting possibility could be positioning one of the RRM domains of PTB1
175 bound to UCUUU sequence of 18S rRNA (PTB1 can bind to UCUUU sequence- *Maris et al 2020*)
176 present at the tip of h16 (528-532 nucleotides) of 18S rRNA. An extra density in the same
177 position is also present in Map A (40S without EMCV IRES or factors- Sup. Fig. 1.2 E) as well,
178 and PTB1 was used as a bait for the pull-down; therefore, this density may be contributed by
179 PTB1-RRM interacting with h16 of 18S rRNA.
180
181 **Table 1: Cryo-EM data and model statistics**

Data collection	**Map A- 40S without factors**	**Map B- 40S-tRNA$_i$-EMCV IRES**	**Map B1- 40S-tRNA$_i$-EMCV IRES-eIF2α-eIF2γ**
Microscope	Talos Arctica		
Camera	Gatan K2 Summit Direct Detector		
Magnification	36000X		
Voltage (kV)	200		
Electron dose (e^-/Å^2)	50-55		
Defocus range	-2 to -0.5		
Pixel size (Å)	1.17		
Number of micrographs	22549		
Cryo-EM reconstruction			
Final number of particles	125503	55231	28439
Point group symmetry	C1	C1	C1
Fsc threshold	0.143	0.143	0.143
Map overall resolution (Å)	4.51	4.55	5.01
Resolution metric	Gold-Standard FSC	Gold-Standard FSC	Gold-Standard FSC
Sharpening B factor(Å^2)	-153.5	-117.9	-122.3
Atomic model refinement			
Resolution (0.5) (Å)	5.0	5.4	6.0
D FSC model (0/0.143/0.5)	4.4/4.5/5.0	4.4/4.5/5.4	4.9/4.9/6.0
Initial models used	6YAN	6YAN; 8OZ0	6YAN; 8OZ0
CC overall			
CC(mask)/(box)/(peaks)/(volume)	0.73/0.83/0.72/0.66	0.77/0.84/0.71/0.77	0.78/0.84/0.72/0.78
Molprobity score	2.3	2.28	2.23

Clash score	19.08	19.09	18.64
No. of atoms/ No. of residues			
Chains	39	41	39
Total atoms (Hydrogens:0)	76455	80057	83717
No. of residues- Proteins/Nucleotides	4916/1744	4918/1912	5660/1912
Bond (RMSD) Lengths (Å)	0.002	0.003	0.003
Bond (RMSD) Angles (^{o})	0.658	0.650	0.659
Ramachandran plot (%)			
Outliers	0.21	0.27	0.20
Allowed	8.94	8.21	7.09
Favored	90.86	91.52	92.72
Rotamer outliers (%)	0.02	0.02	0.00
Cβ outliers (%)	0.00	0.00	0.00
CaBLAM outliers (%)	6.09	5.82	5.47

182

183 2. The EMCV IRES-48S PIC is trapped in a closed conformation

184

185 In EMCV IRES, A-834-U-835-G-836 (AUG-834) forms the start codon *(Kaminski et al 1994;*
186 *Hellen and Wimmer 1995; Pestova et al 1996).* Previous experiments based on toeprints of
187 EMCV IRES-48S PIC assembly suggested A-826-U-827-G-828 (AUG-826) as the codon where
188 48S PIC can assemble, and AUG-834 as the start codon (*Pestova et al 1996*). Furthermore, the
189 intensity of the toeprint at AUG-834 was much higher than at AUG-826 (*Pestova et al 1996;*
190 *Sweeney et al 2014*). Also, AUG-834 is present in a Kozak context (CRCCaugG; R is a purine)
191 *(Kozak 1989)*, where the -3 position is A-831 and +4 is G-837 (Sup. Fig. 2 D), whereas AUG-826
192 is present in a poor Kozak context. In this work, the EMCV IRES construct used has both AUG-
193 826 and AUG-834. Based on the above-mentioned reports, poor and strong Kozak context of
194 AUG-826 and AUG-834, respectively, and placement of AUG-834 at the P site in EMCV IRES-
195 40S binary complex (*Chamond et al 2014*), we reason AUG-834 to base-pair with the
196 anticodon in EMCV IRES-48S PIC (Fig. 2 A), and the flanking nucleotide residues were added
197 as per the sequence (Sup. Fig. 2 D). The recognition of the start codon at the P-site by $tRNA_i$
198 leads to accommodation of ternary complex, and 48S PIC adopts a P_{IN} state in contrast to P_{OUT}
199 state observed during scanning *(Llacer et al 2015; Llacer et al 2021; Yi et al 2022; Petrychenko*
200 *et al 2024)*. A distinct difference of ~7.0 Å could be seen by comparing the $tRNA_i$ position of
201 EMCV IRES-48S PIC with that in the open state (Fig. 2 B), depicting a P_{IN} state of $tRNA_i$. The
202 entrapment of the start codon in the P-site also evokes closure of the mRNA latch formed by
203 18S rRNA helices- h34 of 40S head and h18 of body (*Hussain et al 2014; Llacer et al 2015;*

204 *Hinnebusch 2017*). The h34 of 18S rRNA of EMCV IRES-48S PIC is shifted by 9 Å as compared
205 to the human canonical open state 48S PIC (PDB Id- 7QP6, *Yi et al 2022*). This conformation of
206 18S rRNA correlates well with that of closed 48S PIC (PDB Id- 7QP7, *Yi et al 2022*), suggesting
207 EMCV IRES-48S PIC was captured in a closed state (Fig. 1 C). This closed conformation locks
208 the mRNA in the channel formed within 40S head and body. On the other hand, the
209 conformation of 18S rRNA in Map A (40S ribosome without initiation factors) shows an open
210 state (Sup. Fig. 2 E). The transition from open (PDB Id- 7QP6) to closed states (PDB Id- 7QP7)
211 structures is also accompanied by an upward shift of N terminal domain of eS17 (connecting
212 the head to body) by ~10 Å (*Yi et al 2022*). The EMCV IRES-48S PIC structure correlates with
213 the conformation of eS17 in the human 48S-closed PIC, that is, eS17 N-terminal helix
214 associated with the ribosomal head shifts upward by ~10 Å, keeping C-terminal domain
215 position constant (Fig. 2 D; Sup. Fig. 2 F).
216
217 3. The IRES density connecting 40S head to $tRNA_i$ is contributed by the I domain apical part
218
219 In EMCV IRES-48S PIC complex, we observed a density, likely for double-stranded RNA,
220 connecting 40S head to the $tRNA_i$ elbow region (Fig. 3 A). The extra density interacts with the
221 elbow region and acceptor stem of $tRNA_i$ and ribosomal proteins- uS19 (RPS15) and uS13
222 (RPS18) (Nomenclature- *Ban et al 2014)*. The EMCV IRES contains 4 major stem-loops (H-L)
223 in the functional IRES region (Fig. 3 B) *(Hellen and Wimmer 1995)*. Among these, domains H
224 and I have been shown to interact with 40S *(Chamond et al 2014)* and mutations of conserved
225 residues in these domains severely compromise translation on EMCV IRES *(López de Quinto*
226 *and Martínez-Salas 1997; Hellen and Wimmer 1995)*. Moreover, incubation of Foot and
227 Mouth Disease Virus (FMDV) IRES, an EMCV-like type 2 IRES, with 40S ribosomes has shown a
228 decrease in SHAPE reactivity in its domain 3 apex (*Lozano et al 2018*), which corresponds to
229 EMCV IRES domain I apex. We reasoned that domains H and I may contribute to the double-
230 stranded RNA density emanating from 40S head. The density architecture (Fig. 3 C) could be
231 interpreted as a long main stem (S1) extending away from 40S where the base is anchored to
232 the ribosome by two branches (B1 and B2), and to $tRNA_i$ by one branch (B3), further divided
233 into two sub-branches (B3a and B3b). Visualizing the IRES RNAfold determined-secondary
234 structure (Fig. 3 D- which correlates with the experimental structure proposed in *Duke et al*
235 *1992*), this architecture could be contributed by the apical part of domain I.

236 To determine the tertiary structure of the domain I apex, the IRES region from nucleotide 507-
237 619 was modelled using Alphafold3 (Sup. Fig. 3.1 A). The model was decomposed and
238 reconstructed based on the best-fit in the obtained density for the IRES using Chimera and
239 Coot (Sup. Fig. 3.1 A). The final model was generated after multiple rounds of geometry
240 correction and real space refinements (Fig. 3 E). The final model holds a correlation coefficient
241 of 0.8 with respect to the map (Sup. Fig. 3.1 B), where B1 is AAG loop, B2 is CAAA loop, B3a-
242 GCGA loop, B3b- C rich loop1, and S1 is the major double-stranded stem of domain I. The B-
243 factor of the modelled IRES largely ranges from 124 to 200 (Sup. Fig. 3.1 C). To check the
244 possibility of other IRES domains that might contribute to the extra density, Alphafold3 was
245 used to predict the tertiary structure of isolated EMCV IRES domains (Sup. Fig. 3.2 A-J), using
246 sequences as shown in Sup. Table 1. The predicted tertiary structure of domain H or
247 experimental models of domains D to F did not fit in the observed IRES density (Sup. Fig. 3.2
248 K-L). The domain J-K adopts a Y-shaped structure, and placement of its cryo-EM (PDB Id- 8HUJ)
249 or NMR (PDB Id- 2NBX) structure in the density would clash with 40S (Sup. Fig. 3.2 M).
250 Moreover, in context to EMCV IRES-48S PIC, domain J-K binds eIF4G and the location of eIF4G
251 has been mapped close to ES6 of 18S rRNA, located near the left foot 40S ribosome (*Yu et al*
252 *2011*). The domain I apex model in EMCV IRES-48S PIC shows the RAAA and AAG motif
253 contacts uS19 and uS13, and the GNRA loop with $tRNA_i$ (Fig. 4 A). In addition, incubation of
254 EMCV IRES with rabbit reticulocyte lysate (RRL) protected domain I apex regions, including the
255 CAAA loop in the SHAPE reactivity profile (*Maloney and Joseph, 2024*). These interactions with
256 40S head and $tRNA_i$ could be facilitated by the long length and flexible nature of domain I.
257
258 4. The interaction of domain I of EMCV IRES with ribosomal proteins and initiator tRNA
259
260 The domain I is the longest domain in EMCV IRES, which harbours important motifs such as
261 GNRA, RAAA, and C rich, crucial for IRES activity (*Roberts and Belsham, 1997; Fernández-*
262 *Miragall and Martínez-Salas 2003*) and conserved across all cardioviruses (*Hellen and*
263 *Wimmer 1995).* We mutated the GNRA loop and RAAA loop in EMCV IRES and checked for
264 luciferase activity using a firefly *Luciferase* reporter downstream of the wild-type and mutant
265 IRESs. We found a drastic reduction in the luciferase activity in the mutants as compared to
266 that of the wild-type (Sup. Fig. 4 A), which correlates with previous studies that showed the
267 importance of these motifs in regulating IRES activity (*Roberts and Belsham, 1997; López de*

268 *Quinto and Martínez-Salas, 1997; Robertson et al 1999; Fernández-Miragall and Martínez-*
269 *Salas 2003*). Among these, the CAAA and AAG motifs share potential contact sites with uS13
270 and uS19. The alpha helix (100-117 residues) of uS13 contacts the IRES element at the B3
271 stem (connecting the GNRA loop to RAAA loop) (Fig. 4 B). uS19 contacts the IRES majorly at
272 its CAAA motif through multiple sites involving N-terminal residues, residues- 67 to 75, and C-
273 terminal-102 to 124 (Fig. 4 C). These regions of uS13 and uS19 are rich in basic residues, which
274 might interact with the negatively charged backbone of the IRES element (Fig. 4 B-C). The role
275 of uS13 and uS19 also involves the formation of inter-subunit bridges during 60S joining to
276 form elongation-competent 80S complexes. uS13 interacts with uL5 (RPL11) and uS19 with
277 helix 38 or h38 (1748- 1778, in humans) in 28S rRNA to form inter-subunit bridges- B1b/c and
278 B1a, respectively (Sup. Fig. 4 B) (*Ben-Shem et al 2011; Bowen et al 2015; Khatter et al 2015*).
279 These interactions are dynamic owing to ribosomal subunit rotation and swivelling during 80S
280 ribosomal translocation states (*Khatter et al 2015*).
281
282 On superimposition of 80S ribosomal structure to EMCV IRES-48S PIC model, the IRES density
283 clashes with the position of uL5 and h38 of 28S rRNA (Sup. Fig. 4 C), suggesting repositioning
284 of IRES domain from 40S head during 48S to 80S transition. Interestingly, the h38 residues
285 interacting with uS19 shares considerable similarity in sequence to I domain apex in the EMCV
286 IRES (Fig. 4D), suggesting the domain I apex of EMCV IRES could mimic h38 (60S)-40S
287 interaction (Fig. 4D). The similarity of h38 with the domain I residues provides additional
288 support for annotation of domain I apex in the density.
289
290 The GCGA (GNRA motif- where N is any nucleotide and R is a purine) is known for long-range
291 RNA-RNA interactions, widespread in ribosomal RNA and in some catalytic RNAs. It forms a
292 characteristic U-turn structure (*Fiore and Nesbitt 2013*) and interacts with minor grooves of
293 helical RNA elements (Sup. Fig. 4 D- *Reiter et al 2010*). A single point mutation within this
294 tetraloop (GCGA to GCGC) severely reduced the IRES activity, suggesting its essential for IRES
295 activity (*Roberts and Belsham, 1997; Fernández-Miragall and Martínez-Salas 2003*). The
296 density extending from the elbow region of $tRNA_i$ could fit in the characteristic U-turn,
297 adopted by conventional GNRA motifs. In EMCV IRES, the GNRA motif is represented by GCGA
298 loop, preceded by a C-rich region and in close contact with the $tRNA_i$ elbow and acceptor stem
299 (Fig. 4 E). Thus, we infer that EMCV IRES interacts with $tRNA_i$ by virtue of its GCGA loop.

300 5. The position of eIF2-ternary complex is shifted towards 40S head in EMCV IRES-48S PIC in
301 contrast to canonical 48S PIC
302
303 We could fit eIF2α and eIF2γ in their respective densities in Map B1 (Fig. 5 A). Focussed
304 classification or refinement did not yield any distinct density corresponding to the position of
305 eIF2β, probably due to the flexibility associated with repositioning of eIF2β during transition
306 from open to closed complexes *(Llacer et al 2015; Llacer et al 2021; Yi et al 2022; Petrychenko*
307 *et al 2024)*. Previous reports on EMCV IRES suggested its direct interaction with eIF2 (*Scheper*
308 *et al 1991; Scheper et al 1994*) and inactivation of eIF2 compromises EMCV IRES-mediated
309 translation *(*Welnowska *et al 2011; Kwon et al 2016)*, indicating EMCV IRES's dependence on
310 the canonical ternary complex. Here, we observe a direct interaction of EMCV IRES with
311 ternary complex via $tRNA_i$, a feature not observed in previously determined HCV (*Yamamoto*
312 *et al 2014; Yamamoto et al 2015; Brown et al 2022*) and CrPV IRES-bound ribosomal structures
313 (*Pisareva et al 2018; Acosta-Reyes et al 2019*).
314
315 As found in canonical 48S PICs (*Hashem et al 2013*; *Brito Querido et al 2024; Petrychenko et*
316 *al 2024)*, eIF2α-domain 1 is in close contact with ribosomal protein- uS7, and domain 2 with
317 $tRNA_i$ elbow and domain 3 with eIF2γ in EMCV IRES-48S PIC. The position of eIF2γ and eIF2α-
318 domain 3 (D3) is distinct from mammalian 48S-closed PICs (PDB Id- 6YAN and 7QP7) as we
319 could observe a shift by ~10 Å towards the head of 40S on superimposing the 18S rRNA from
320 EMCV IRES 48S PIC and mammalian late-stage 48S PIC (Fig. 5 B). The ternary complex is
321 flexible, and it moves away from ribosomal head towards the body on recognition of
322 authentic start codon as studied in yeast (*Villamayor-Belinchón et al 2024*) and human
323 (*Petrychenko et al 2024)*. This opposite directional shift of the ternary complex in the EMCV
324 IRES-48S PIC is evident in $tRNA_i$ acceptor stem as well (Fig. 5 C). This shift could be due to the
325 rigid stem B3 (consisting G-C base pairs), connecting 40S head to GNRA loop, which interacts
326 with the $tRNA_i$ at its elbow and acceptor arm, and the association of eIF2α-D3 and eIF2γ with
327 the acceptor arm of $tRNA_i$ orchestrated with the conformational change.
328
329 During the transition of 48S PIC to 80S elongation-competent complex, there are major
330 changes in the conformation of $tRNA_i$ due to the joining of eIF5B, and release of eIF2
331 (*Petrychenko et al 2024*). This joining event of eIF5B positions the $tRNA_i$ elbow and acceptor

332 stem towards the 40S body to aid 60S ribosomal subunit joining (*Petrychenko et al 2024*).
333 However, in the context of EMCV IRES-48S PIC, we have seen the positioning of $tRNA_i$ elbow
334 and acceptor stem towards the 40S head, away from the body (Fig. 5 C). On superimposing
335 the human 48S PIC structure (before 60S joining), 48S-5 (PDB Id- 8PJ5- *Petrychenko et al 2024*),
336 we could see that $tRNA_i$ in EMCV IRES-48S PIC is away from the canonical $tRNA_i$ position (in
337 contact with eIF5B) (Fig. 5 D). Therefore, we anticipate a change in $tRNA_i$ conformation during
338 eIF5B joining and eIF2 release. Furthermore, the IRES (domain I) interacting with the $tRNA_i$
339 elbow needs to be displaced from the position to facilitate the interaction of $tRNA_i$ with
340 eIF5Band this rearrangement would also aid in 60S joining and avoid steric clash with the IRES
341 domain I.

342

343 **Discussion:**

344

345 The mechanism of IRES recruitment on 40S ribosome varies considerably among different
346 types of IRESs. CrPV intergenic IRES binds to 40S ribosome by mimicking tRNA-mRNA
347 interaction with the help of pseudoknot 1 *(Petrov et al 2016; Fernandez et al 2014; Murray et*
348 *al 2016; Acosta-Reyes et al 2019)*, whereas HCV IRESs associates with the solvent side of 40S
349 body by replacing eIF3 with its domain 3 *(Spahn et al. 2004; Hashem et al 2013; Niepmann*
350 *and Gerresheim 2020; Brown et al 2022)*. In this study, we capture EMCV IRES in 48S PIC
351 context, interacting with 40S ribosomal head and $tRNA_i$. Model building suggests that domain
352 I of EMCV IRES interacts with 40S ribosome head and $tRNA_i$ elbow stem (Fig. 6 A). The
353 similarity in the sequence of h38 of 28S rRNA with the domain I and its ability to interact with
354 uS19-N terminal via RAAA motif (*Khatter et al 2015*) suggests a mimicry mechanism adopted
355 by EMCV IRES for its recruitment to the ribosome. Moreover, the conservation of domain I
356 apex sequence and motifs (RAAA, AAG loop, C-rich and GNRA) across Cardioviruses- Theiler's
357 murine Encephalitis virus (TMEV), Vilyuisk human encephalomyelitis virus (VHEV), Theiler's-
358 like rat virus (TRV) and Saffold viruses 1 and 2 (SAFV-1 and SAFV-2) and Apthoviruses (AAG
359 loop is replaced by ACG loop)- Foot and mouth disease virus (*Hellen and Wimmer 1995; Liang*
360 *et al 2008*) suggests that these IRESs might adopt similar strategies for 48S formation (Fig. 6
361 B-C). Like EMCV IRES, the type 1 IRES (Poliovirus, Coxsackie virus, etc.) also harbours the GNRA
362 loop, preceded by a C-rich loop at its longest domain, known for long-range RNA-RNA

363 interactions. The segment harbouring GNRA loop is highly conserved across the type 1 family
364 of IRESs (*Kim et al 2015*). The domain I of EMCV IRES is similar to domain IV of polioviral IRES
365 or other type 1 IRESs in terms of length, secondary structure, and conserved motifs (GNRA,
366 C-rich) positioning (Fig. 6 C). Therefore, we anticipate a similar interaction of domain IV (in
367 type 1 IRES class) with $tRNA_i$. Also, this interaction of IRES with $tRNA_i$ could be a strategy by
368 which these IRESs can sequester the $tRNA_i$ pool in the cell, rendering them unavailable for
369 capped cellular mRNAs. During the revision of this work, a preprint reported a structure of
370 polioviral IRES-48S PIC (*Velazquez et al 2025*), which shows that domain IV apex (similar to
371 domain I apex in EMCV IRES) interacts with uS13 and uS19, and the GNRA loop directly
372 interacts with $tRNA_i$ during start codon recognition (*Velazquez et al 2025*) as observed in
373 EMCV IRES-48S PIC. Similarly, the Aichi viral IRES (type 5- *Abdullah et al 2023*) harbours a GNRA
374 loop in its longest domain, which is domain J. Deletion of the GNRA loop compromises the
375 IRES activity; however, substitution mutations in this region either elevate the IRES activity or
376 it remains unaltered (*Yu et al 2011*). We hypothesize that Aichiviral IRES might use this motif
377 to mediate long-range interactions with tRNAi, similar to type 1 and type 2 IRESs, as all these
378 IRESs require eIF2-ternary complex for the formation of 48S PIC.
379
380 The EMCV IRES does not require scanning, and the start codon (A-834) is directly placed in
381 the P site, which would eventually place the domain L at the mRNA exit site, preceded by
382 domain J-K that interacts with eIF4G-eIF4A (Fig. 6 A). Earlier, biochemical studies suggested
383 eIF4G to be positioned close to ES6 of 18S rRNA in EMCV IRES-bound 48S PIC (*Yu et al 2011*).
384 The human 48S PIC with a 5' capped mRNA showed a similar location for eIF4G, that is at the
385 mRNA exit site contacting eIF3 (*Brito Querido et al 2020; Brito Querido et al 2024)*. Locating
386 eIF4F has been challenging due to the inherent flexibility associated with the eIF4F complex
387 on mRNA and requires association with eIF3 in canonical 48S context (*Brito Querido et al*
388 *2020; Brito Querido et al 2024)*. However, the canonical eIF3-eIF4G interaction (Villa et al
389 2013) is dispensable for EMCV IRES-48S PIC formation (Lomakin et al 2000; Sweeney et al
390 2014), and no density for eIF3 was observed even after focused classification. However, after
391 the initial submission of this work, a preprint reported a structure of reconstituted EMCV IRES-
392 48S PIC where eIF3 is present at the canonical position (*Bhattarcharjee et al 2025*). This
393 position of eIF3 suggests the possibility that eIF4G-eIF4A proteins could be placed similarly to
394 the canonical eIF3-eIF4G-eIF4A position (*Brito Querido et al 2024*) in context to EMCV IRES-

395 48S PIC. Thus, placing eIF4G-domain J-K close to ES6 of 40S ribosome, which coincides with
396 the previous hydroxyl radical cleavage assay (*Yu et al 2011*). In addition to initiation factors,
397 the ITAF- PTB1 serves as an essential ITAF for 48S PIC formation on EMCV IRES, but the
398 obtained map shows no distinct density to PTB1. PTB1 binds to the base of domains H and I,
399 and domain K loop (*Kafasla et al 2009; Dorn et al 2023*), and the flexibility associated with
400 these domains might have hindered capturing of PTB1 in the reported 48S complex (Fig. 6 A).
401 However, the unassigned extra density at the mRNA entry site could be contributed by PTB1-
402 RRM interacting with 18S rRNA, as discussed previously.
403
404 The structural studies on type 2 IRESs have been limited due to their flexible nature. In the
405 cryo-EM map and structural analysis presented here, we could capture a part of EMCV IRES
406 in 48S context (Fig. 6 A) and fetch a significant understanding of ribosomal recruitment by
407 EMCV IRES and 48S PIC formation. As mentioned above, the cryo-EM map of reconstituted
408 EMCV IRES-48S PIC (*Bhattarcharjee et al 2025*) show similar findings, where the density for
409 the apical portion of domain I of the IRES is only observed and it interacts with uS13 and uS19
410 on 40S ribosome, and $tRNA_i$. A higher resolution of the reconstituted EMCV IRES-48S PIC (3.2
411 Å) helped the authors to identify interactions of individual IRES nucleotides with their binding
412 partners (*Bhattarcharjee et al 2025*). In future, the entrapment of additional factors would
413 significantly provide more insights into EMCV IRES 48S PIC. The conservation of secondary
414 structures and motifs such as GNRA within the picornaviruses (type 1, 2, and Aichiviral IRESs)
415 suggests common strategies of interaction in the context of 48S PICs in the Picornaviridae
416 family.
417
418 **Materials and Methods:**
419
420 1. Plasmid constructs and Molecular Cloning
421 EMCV IRES 905 was obtained from EMCV-L plasmid- EMCV IRES (nt 280–905) into pCR2.1 and
422 inserted in pcDNA3.1 using BamHI and XbaI restriction sites. Polypyrimidine tract binding
423 protein 1 was cloned from HEK293 cDNA, and 3C protease site (LEVLFQGP) was inserted at
424 the N-terminal and inserted into pET28a in between BamHI and HindIII restriction sites,
425 retaining the N-terminal 6X Histidine tag.

426 EMCV IRES-Luciferase constructs- The firefly luciferase gene was inserted downstream of
427 EMCV IRES in-frame with A-834 residue of IRES to generate the wild-type EMCV IRES-
428 Luciferase construct in pcDNA3.1 (WT-Luc). The CAAAA (RAAA) loop and GCGA (GNRA) loop
429 were mutated to GCTGA and TACG, as per functional assay reports for FMDV IRES and EMCV
430 IRES to generate RAAAmut-Luc and GNRAmut-Luc, respectively (*López de Quinto and*
431 *Martínez-Salas, 1997; Fernández-Miragall and Martínez-Salas, 2003*). The sequence of oligos
432 or primers used is listed in Sup. Table 2.
433
434 2. Protein overexpression and purification
435 PTB1 (Histidine tag- 3Cprotease site- *PTB1* gene) was overexpressed using 0.5 mM IPTG in *E.*
436 *coli* BL21 cells at 30 ^{o}C, 120 rpm for 4 hours in Luria broth. 2 l harvested culture was lysed
437 using Buffer N1 (20 mM HEPES pH-7.4, 300 mM KCl, 2 mM $MgCl_2$, 10 % glycerol, 10 mM
438 imidazole, 5 mM β-mercaptoethanol, 0.05 % Triton-X-100, 2 mM PMSF) and sonicated at 18
439 % amplitude, 10 s ON and 20 s OFF pulses, 30 cycles and centrifuges at 20000 rpm for 20
440 minutes and the supernatant was loaded on Ni-NTA column and eluted using a gradient of N1
441 to N2 buffer (20 mM HEPES pH-7.4, 300 mM KCl, 2 mM $MgCl_2$, 10 % glycerol, 500 mM
442 imidazole, 5 mM β-mercaptoethanol). PTB1 was eluted at 250 mM Imidazole concentration.
443 The eluant fractions (diluted to 100 mM KCl) were further loaded on Heparin column and
444 eluted by applying a gradient of 100 mM to 1000 mM KCl. The protein was eluted at 250 mM
445 KCl concentration. The eluant fractions were stored at -80 ^{o}C after Size Exclusion
446 Chromatography in Buffer S (20 mM HEPES pH-7.4, 200 mM KCl, 2 mM $MgCl_2$, 5 % glycerol, 1
447 mM DTT) at 2.5 mg/ml.
448 3C protease was overexpressed using 0.5 mM IPTG in *E. coli* BL21 cells at 30 ^{o}C, 120 rpm in
449 Luria broth. 2 l harvested culture was lysed using Buffer N11 (20 mM HEPES pH-7.4, 200 mM
450 KCl, 2 mM $MgCl_2$, 10 % glycerol, 10 mM imidazole, 5 mM β-mercaptoethanol, 0.05 % Triton-
451 X-100, 2 mM PMSF) and sonicated at 18 % amplitude, 10 s ON and 20 s OFF pulses, 30 cycles
452 and centrifuges at 20000 rpm for 20 minutes and the supernatant was loaded on Ni-NTA
453 column and eluted using a gradient of N11 to N22 buffer (20 mM HEPES pH-7.4, 200 mM KCl,
454 2 mM $MgCl_2$, 10 % glycerol, 500 mM imidazole, 5 mM β-mercaptoethanol). 3C protease was
455 eluted at 250 mM imidazole concentration. The eluant fractions were subjected to Size
456 Exclusion Chromatography in Buffer S (20 mM HEPES pH-7.4, 100 mM KOAc, 2 mM $MgCl_2$, 10
457 % glycerol, 1 mM DTT), and peak fractions were concentrated and stored at 2.5 mg/ml.

458 3. *In vitro* transcription of EMCV IRES

459 EMCV IRES 905-pcDNA3.1 was linearized using Xba1 restriction enzyme and transcribed using
460 Promega-RiboMAX™ Large Scale RNA Production Systems as per manufacturer's protocol. 1
461 µg of linearized plasmid yielded 87 µg of RNA after DNase treatment and RNA cleanup (RNA
462 clean up kit- NEB). WT-Luc, GNRAmut-Luc, and RAAAmut-Luc were linearized using XhoI and
463 transcribed *in vitro* using the same strategy.

464

465 4. Assembly of EMCV IRES 48S PIC using Talon Affinity Chromatography

466 12 µg of IRES was heated at 95 ^{o}C to dissolve any secondary structures acquired and refolded
467 using buffer R (20 mM HEPES pH-7.4, 150 mM KOAc, 2 mM $MgCl_2$, 2 mM β-mercaptoethanol,
468 0.25 mM spermidine) at 37 ^{o}C for 5 minutes, and PTB1 (1:2 = IRES: PTB1) was added and
469 further incubated at 30°C for 5 minutes. Simultaneously, Rabbit Reticulocyte Lysate (RRL)
470 (Promega) was incubated at 30°C with ATP, Amino acid mix minus Leucine, murine RNase
471 Inhibitor for 5 minutes, and then mixed with the IRES-PTB1 vial with instant addition of 6 mM
472 GMP-PnP per reaction (100 µl) and incubated at 30 ^{o}C for 8 minutes, followed by ice
473 incubation. The reaction was loaded onto Talon beads equilibrated with Buffer A (20 mM
474 HEPES, pH 7.4, 150 mM KOAc, 2 mM MgCl2, 4% glycerol, 5 mM imidazole, 2 mM β-
475 mercaptoethanol). After recommended passes, reloading and incubation, the flow through
476 was collected and the beads were washed with Buffer A until A260 attains a baseline value
477 (~0), following which 3C protease in Buffer A was added to the beads and left for overnight
478 incubation. Fractions were eluted using Buffer A (400 µl each in 10 vials) and subjected to
479 analysis such as A260 measurements and agarose gel electrophoresis. Samples having the
480 RNA bands were pelleted using a 1ml sucrose cushion (20 mM HEPES pH-7.4, 150 mM KOAc,
481 2mM $MgCl_2$, 30% Sucrose, 1mM DTT) in SW60 tubes and centrifuged at 50,000 rpm for 10
482 hours at 4 ^{o}C. The pellet was resuspended in 20 µl buffer R and used for Cryo-EM grid
483 preparation (no crosslinker was used to avoid artifacts).

484

485 5. Negative stain analysis and Mass Spectrometry

486 The final sample was diluted 10 times using buffer R and applied on 400-mesh Cu TEM grids,
487 which were freshly glow-discharged (negative polarity) for 30 s in GloQube glow-discharge
488 system, stained using 1% Uranyl acetate solution, and analysed using Talos L120C transmission
489 electron microscope at 57000 X magnification. Furthermore, the sample was digested by

trypsin and subjected to NanoOrbitrap analysis for the identification of proteins in the complex.

6. Cryo-EM sample preparation

3 µl of resuspended pellet (2.96 A260) was applied on glow-discharged Quantifoil R 1.2/1.3 300 mesh 2nm Carbon Coated Grid and Blotted using 8s and 8.5s Blot time, zero Blot force at 16°C and 100% Humidity, and plunged into liquid ethane. Cryo-EM data were collected on Talos Arctica transmission electron microscope equipped with a FEG at 200 kV (Thermo Fisher Scientific). All data were collected using a Gatan K2 Summit Direct Detector at a nominal magnification of 36,000 X, and a pixel size of 1.17 Å with a total electron dose of 55 e- /Å2 fractionated over 20 frame movies with a dose rate of ~2.5 e-/Å^2 /frame.

6. Data Processing

Micrographs were collected and processed using CryoSPARC v3.3 (*Punjani et al 2017*). The micrographs were patch motion corrected and CTF was estimated. Using a blob picker with an average diameter of 300 Å particles were picked and extracted. The extracted particles were subjected to multiple rounds of 2D classification. Final 2D classes showing promising ribosome 2D features were selected for *ab initio* reconstruction. The junk was discarded, and the 237054 good particles were classified into 2 classes using a mask around tRNA$_i$. We obtained 2 classes- Empty 40S (1.25L particles- Class 1 or Map A), and 40S with tRNA bound (1.11L particles- Class 2). Class 2 was further classified into 2 classes using a 3D mask around the IRES density and subjected to non-uniform refinement with global CTF refinement to yield Map B, having tRNA$_i$ and IRES density (55k particles). This was subjected to Non-uniform Refinement (*Punjani et al 2020*) with global CTF refinement. Map B class was further classified using a mask around eIF2α and eIF2γ to yield 2 classes- 40S-tRNA$_i$-IRES-eIF2 (28k particles- Map B1) and 40S-tRNA$_i$-IRES (26k particles). The obtained maps were then subjected to model building and refinement. The local resolution for the obtained maps were estimated using Phenix (*Liebschner et al 2019).*

521 7. Map analysis and Model building

522 To the obtained maps, 40S ribosome (PDB Id- 6YAN) was fitted using UCSF Chimera. The 40S
523 head (Head proteins + 18S rRNA (1197-1688) + eS17) and 40S body (Body proteins + 18S rRNA
524 (1-1196; 1689-1870)) was fitted to the obtained maps separately and subjected to Rigid Body
525 Fit and Real Space Refinement using PHENIX *(Liebschner et al 2019)*. The models were merged
526 using Coot *(Emsley et al 2010)* and subjected to Real Space Refinement. $tRNA_i$ and mRNA
527 models were taken from PDB Id- 8OZ0 and fitted to the maps- B and B1 in Chimera. eIF2α and
528 eIF2γ from PDB Id- 8OZ0 were rigid-body fitted to Map B1 and then mutated as per Rabbit
529 eIF2 protein sequence (NCBI Reference Sequence- XP_002719561.1; XP_051683593.1) and
530 subjected to a final Real Space Refinement. The IRES I domain apex model was predicted from
531 Alphafold3 (*Abramson et al 2024*) and the helical sub-domains were dismantled and fitted
532 according to best fit using Chimera, followed by chain joining in Coot with manual Real Space
533 Refinement (*Afonine et al 2018*). The geometry was corrected using Geometry minimization
534 tool in Phenix with rounds of Real Space Refinement. H domain model was predicted using
535 Alphafold3. The final model yielded 40S-EMCV IRES-$tRNA_i$ (Map B) and 40S-EMCV IRES-$tRNA_i$-
536 eIF2αϒ (Map B1). All the figures were made using ChimeraX *(Pettersen et al 2021).* The models
537 were real space refined using Phenix, and the Fourier Shell Correlation for 'Map to Model' for
538 each was determined at 0.5 FSC (Sup. Fig. 2A-C; Table 1).

539

540 8. Luciferase assay

541 WT-Luc, GNRAmut-Luc, and RAAAmut-Luc RNA was subjected to polyadenylation using *E.*
542 *coli* Poly(A) Polymerase and ATP supplied in New England Biolabs kit using manufacturer's
543 protocol. Post polyadenylation, the RNA was extracted using RNA cleanup kit (NEB). The RNA
544 was denatured at 95 ^{o}C and refolded using buffer R at 37 ^{o}C for 5 minutes. To 1 µg of RNA, 10
545 µl RRL was added with 0.25 µM amino acid mix minus leucine, and amino acid mix minus
546 methionine, 1 mM ATP, 0.5 mM GTP, and the remaining volume was adjusted using buffer R
547 to a final volume of 30 µl. Each reaction was divided into 3 sets- 10 µl each and incubated at
548 30 ^{o}C for 3 hours. The luciferase activity in each reaction was measured by adding 10 µl of
549 Steady-Glo Luciferase reagent (Promega) and quantified using a Tecan plate reader. The
550 graphs were plotted using Graphpad prism.

551

9. Secondary Structure Determination and Multiple Sequence Alignments

The secondary structure for I domain apex was obtained from RNAfold (*Gruber et al 2008*). Multiple sequence alignments were performed using Clustal Omega (*Sievers et al 2021*). Sequence accession number for various sequence used- EMCV (NC_001479.1), FMDV (NC_039210.1), TMEV (DQ401688.1), TRV (AB090161.1), VHEV (M80888.1), SAFV (FM207487.1), Poliovirus (NC_002058.3).

Accession codes:

Maps and atomic coordinates of the 40S ribosome (Map A), 40S ribosome-EMCV IRES-$tRNA_i$ (Map B) and 40S ribosome-EMCV IRES-ternary complex (Map B1) have been deposited in the EMDB database with accession codes- EMD-64646, EMD-64644, and EMD-64645, respectively and in the PDB database with accession code- 9UZM, 9UZK, and 9UZL, respectively.

Acknowledgements:

EMCV IRES (nt 280–905) into pCR2.1 was a kind gift from Dr. Bruno Sargueil, CNRS UMR8015, Universit´e Paris Descartes, France and 3C protease-pET24 was a kind gift from Prof. Raghavan Varadarajan, Indian Institute of Science (IISc), India. We thank various central facilities, namely Cryo-EM, Mass Spectrometry and Computational cluster at the Division of Biological Sciences, IISc for support. DD acknowledges the DBT-JRF Programme for fellowship. The authors acknowledge the DST-FIST support to the department. This work was supported by the Intermediate Fellowship from DBT-Welcome Trust India Alliance to TH (IA/I/17/2/503313).

Conflict of Interest:

The authors declare no conflict of interest

586 **Figure legends:**
587
588 **Figure 1 (A)** Different views of EMCV IRES-48S PIC (Map B1) by 45° rotation along one axis.
589 The map shows densities assigned to 40S ribosome, RNA (in channel), ternary complex and
590 IRES density at the inter-subunit region of head. **(B)** View of Map B and zoomed view of
591 densities corresponding to IRES and $tRNA_i$.
592
593 **Figure 2 (A)** Fitting of $tRNA_i$-base paired to start codon AUG (left). Zoomed view of codon-
594 anticodon interaction (middle), and B-factor for codon-anticodon interaction (right). **(B)** The
595 $tRNA_i$ in EMCV IRES-48S PIC is in P_{IN} state similar to that in human 48S PIC P_{IN} state (PDB Id-
596 7QP7) and its anticodon shows ~7 Å shift as compared to human 48S PIC open state (PDB Id-
597 7QP6). **(C)** Comparison of ribosomal conformation (18S rRNA) of EMCV IRES 48S PIC with
598 Human open and closed state (PDB Id- 7QP6 and 7QP7, respectively). Focusing on the entry
599 site and the helices governing latch conformation- Helix 34 moves toward helix 18 by 9 Å. **(D)**
600 Movement of eS17 in open and closed states of ribosome. Zoomed view of comparison
601 between eS17 in EMCV IRES 48S PIC and Human 48S PIC open state- showing an upward shift
602 of the N-terminal domain by ~10 Å.
603
604 **Figure 3 (A)** Extra density connecting the head of 40S to $tRNA_i$ elbow region is contributed by
605 EMCV IRES RNA in Map B1. Rotated views of RNA density showing its connection to the 40S
606 head via uS13 and uS19 and to $tRNA_i$ via its elbow region. **(B)** Organization of EMCV IRES
607 domains from D-L, where H-L makes the functional IRES moiety (*Hellen and Wimmer et al*
608 *1995*). **(C)** Deciphering the architecture of the obtained IRES density. The density could be
609 interpreted as a long main stem (S1) extending away from the ribosome, where the base is
610 anchored to the ribosome by two branches (B1 and B2), and to $tRNA_i$ by one branch (B3),
611 further divided into two sub-branches (B3a and B3b). **(D)** Secondary structure of apical region
612 of domain I (made using RNAfold) marking the Stem and branches, along with imported
613 loops. **(E)** Fitting of domain I apex in the density (Rotated views). The sub-domains are
614 coloured as proposed in Fig 3C-D.
615
616 **Figure 4 (A)** Model showing connections of domain I apex with uS13, uS19, and $tRNA_i$. **(B)**
617 uS13 interacts with B3 branch or sub-domain of IRES via its alpha helix (100-117 residues). **(C)**
618 Multiple point of contacts between uS19 and domain I motifs- RAAA and AAG. The
619 electrostatic potential map of uS19 suggests that EMCV IRES interacts via ionic interactions
620 with its phosphate backbone. **(D)** Sequence alignment of h38 with domain I apex of EMCV
621 IRES showing sequence identity. Overlapping of uS19 from 80S (PDB Id- 4UG0) and EMCV
622 IRES-48S PIC show that the interaction of uS19 with EMCV IRES is similar to interaction with
623 that of h38. **(E)** The fit of GNRA or GCGA stem and its contact with $tRNA_i$ at the elbow region
624 and acceptor stem.
625
626 **Figure 5 (A)** Inter-subunit view of EMCV IRES 48S PIC showing position for ternary complex on
627 map. Fitting of eIF2α and eIF2γ in its corresponding density in Map B1. **(B)** Overlapping EMCV
628 IRES 48S PIC on mammalian late-stage 48S PIC (PDB Id- 6YAN), indicates a shift in position of
629 eIF2γ towards 40S head. **(C)** Zoomed view showing the positions of eIF2γ, tRNAi, and eIF2α in
630 the EMCV IRES 48S PIC relative to those in the mammalian late-stage 48S PIC (PDB ID 6YAN).
631 The black arrow indicates the shift in position. **(D)** Superimposition of the EMCV IRES-48S PIC
632 on the human late-stage 48S PIC (before 60S joining; PDB Id- 8PJ5), showing the conformation

633 of $tRNA_i$ in association with eIF2 and IRES and $tRNA_i$ with eIF5B in the canonical context,
634 respectively. (right) Zoomed view of $tRNA_i$ conformation in both complexes.
635
636 **Figure 6 (A)** EMCV IRES secondary structure depicting the role of binding partners for each
637 domain in context to translation initiation. The known tertiary structure of EMCV IRES and its
638 binding partners are depicted. The domains responsible for binding PTB1 are boxed. **(B)**
639 Conservation of domain I apex sequence and secondary structure across type 2 IRES family.
640 **(C)** Comparison of secondary structure of EMCV and FMDV IRES to that of Polioviral IRES (type
641 1).
642
643 **References:**
644
645 Abaeva IS, Young C, Warsaba R, Khan N, Tran LV, Jan E, Pestova TV, Hellen CUT. The structure
646 and mechanism of action of a distinct class of dicistrovirus intergenic region IRESs. Nucleic
647 Acids Res. 2023 Sep 22;51(17):9294-9313. doi: 10.1093/nar/gkad569. PMID: 37427788;
648 PMCID: PMC10516663.

649 Abdullah SW, Wu J, Wang X, Guo H, Sun S. Advances and Breakthroughs in IRES-Directed
650 Translation and Replication of Picornaviruses. mBio. 2023 Apr 25;14(2):e0035823. doi:
651 10.1128/mbio.00358-23. Epub 2023 Mar 20. PMID: 36939331; PMCID: PMC10127998.

652 Abramson J, Adler J, Dunger J, Evans R, Green T, Pritzel A, Ronneberger O, Willmore L, Ballard
653 AJ, Bambrick J, Bodenstein SW, Evans DA, Hung CC, O'Neill M, Reiman D, Tunyasuvunakool K,
654 Wu Z, Žemgulytė A, Arvaniti E, Beattie C, Bertolli O, Bridgland A, Cherepanov A, Congreve M,
655 Cowen-Rivers AI, Cowie A, Figurnov M, Fuchs FB, Gladman H, Jain R, Khan YA, Low CMR, Perlin
656 K, Potapenko A, Savy P, Singh S, Stecula A, Thillaisundaram A, Tong C, Yakneen S, Zhong ED,
657 Zielinski M, Žídek A, Bapst V, Kohli P, Jaderberg M, Hassabis D, Jumper JM. Accurate structure
658 prediction of biomolecular interactions with AlphaFold 3. Nature. 2024 Jun;630(8016):493-
659 500. doi: 10.1038/s41586-024-07487-w. Epub 2024 May 8. PMID: 38718835; PMCID:
660 PMC11168924.

661 Acosta-Reyes F, Neupane R, Frank J, Fernández IS. The Israeli acute paralysis virus IRES
662 captures host ribosomes by mimicking a ribosomal state with hybrid tRNAs. EMBO J. 2019 Oct
663 4;38(21):e102226. doi: 10.15252/embj.2019102226. Epub 2019 Oct 14. PMID: 31609474;
664 PMCID: PMC6826211.

665 Afonine PV, Poon BK, Read RJ, Sobolev OV, Terwilliger TC, Urzhumtsev A, Adams PD. Real-space
666 refinement in PHENIX for cryo-EM and crystallography. Acta Crystallogr D Struct Biol. 2018 Jun
667 1;74(Pt 6):531-544. doi: 10.1107/S2059798318006551. Epub 2018 May 30. PMID: 29872004;
668 PMCID: PMC6096492.

669 Baglioni C, Simili M, Shafritz DA. Initiation activity of EMC virus RNA, binding to initiation factor
670 eIF-4B and shut-off of host cell protein synthesis. Nature. 1978 Sep 21;275(5677):240-3. doi:
671 10.1038/275240a0. PMID: 211427.

672 Ban N, Beckmann R, Cate JH, Dinman JD, Dragon F, Ellis SR, Lafontaine DL, Lindahl L, Liljas A,
673 Lipton JM, McAlear MA, Moore PB, Noller HF, Ortega J, Panse VG, Ramakrishnan V, Spahn CM,
674 Steitz TA, Tchorzewski M, Tollervey D, Warren AJ, Williamson JR, Wilson D, Yonath A, Yusupov

675 M. A new system for naming ribosomal proteins. Curr Opin Struct Biol. 2014 Feb;24:165-9.
676 doi: 10.1016/j.sbi.2014.01.002. Epub 2014 Feb 10. PMID: 24524803; PMCID: PMC4358319.

677 Ben-Shem A, Garreau de Loubresse N, Melnikov S, Jenner L, Yusupova G, Yusupov M. The
678 structure of the eukaryotic ribosome at 3.0 Å resolution. Science. 2011 Dec
679 16;334(6062):1524-9. doi: 10.1126/science.1212642. Epub 2011 Nov 17. PMID: 22096102.

680 Bhattacharjee S, Abaeva IS, Brown ZP, Arhab Y, Fallah H, Hellen CUT, Frank J, Pestova TV. The
681 mechanism of ribosomal recruitment during translation initiation on Type 2 IRESs. bioRxiv
682 [Preprint]. 2025 Jun 11:2025.06.11.659010. doi: 10.1101/2025.06.11.659010. PMID:
683 40568087; PMCID: PMC12191231.

684 Boehringer D, Thermann R, Ostareck-Lederer A, Lewis JD, Stark H. Structure of the hepatitis C
685 virus IRES bound to the human 80S ribosome: remodeling of the HCV IRES. Structure. 2005
686 Nov;13(11):1695-706. doi: 10.1016/j.str.2005.08.008. PMID: 16271893.

687 Bowen AM, Musalgaonkar S, Moomau CA, Gulay SP, Mirvis M, Dinman JD. Ribosomal protein
688 uS19 mutants reveal its role in coordinating ribosome structure and function. Translation
689 (Austin). 2015 Nov 18;3(2):e1117703. doi: 10.1080/21690731.2015.1117703. PMID:
690 26824029; PMCID: PMC4721500.

691 Brito Querido J, Díaz-López I, Ramakrishnan V. The molecular basis of translation initiation and
692 its regulation in eukaryotes. Nat Rev Mol Cell Biol. 2024 Mar;25(3):168-186. doi:
693 10.1038/s41580-023-00624-9. Epub 2023 Dec 5. PMID: 38052923.

694 Brito Querido J, Sokabe M, Díaz-López I, Gordiyenko Y, Fraser CS, Ramakrishnan V. The
695 structure of a human translation initiation complex reveals two independent roles for the
696 helicase eIF4A. Nat Struct Mol Biol. 2024 Mar;31(3):455-464. doi: 10.1038/s41594-023-
697 01196-0. Epub 2024 Jan 29. PMID: 38287194; PMCID: PMC10948362.

698 Brito Querido J, Sokabe M, Kraatz S, Gordiyenko Y, Skehel JM, Fraser CS, Ramakrishnan V.
699 Structure of a human 48*S* translational initiation complex. Science. 2020 Sep
700 4;369(6508):1220-1227. doi: 10.1126/science.aba4904. PMID: 32883864; PMCID:
701 PMC7116333.

702 Brown ZP, Abaeva IS, De S, Hellen CUT, Pestova TV, Frank J. Molecular architecture of 40S
703 translation initiation complexes on the hepatitis C virus IRES. EMBO J. 2022 Aug
704 16;41(16):e110581. doi: 10.15252/embj.2022110581. Epub 2022 Jul 13. PMID: 35822879;
705 PMCID: PMC9379550.

706 Carocci M, Bakkali-Kassimi L. The encephalomyocarditis virus. Virulence. 2012 Jul 1;3(4):351-
707 67. doi: 10.4161/viru.20573. Epub 2012 Jun 22. PMID: 22722247; PMCID: PMC3478238.

708 Chamond N, Deforges J, Ulryck N, Sargueil B. 40S recruitment in the absence of eIF4G/4A by
709 EMCV IRES refines the model for translation initiation on the archetype of Type II IRESs.
710 Nucleic Acids Res. 2014;42(16):10373-84. doi: 10.1093/nar/gku720. Epub 2014 Aug 26. PMID:
711 25159618; PMCID: PMC4176346.

712 Datey A, Sharma P, Khaja FT, Rahil H, Hussain T. Yeast Eukaryotic Initiation Factor 4B Remodels
713 the MRNA Entry Site on the Small Ribosomal Subunit. Biochemistry. 2025 Feb 4;64(3):600-
714 608. doi: 10.1021/acs.biochem.4c00489. Epub 2025 Jan 23. PMID: 39847343.

715 de Breyne S, Yu Y, Unbehaun A, Pestova TV, Hellen CU. Direct functional interaction of initiation
716 factor eIF4G with type 1 internal ribosomal entry sites. Proc Natl Acad Sci U S A. 2009 Jun
717 9;106(23):9197-202. doi: 10.1073/pnas.0900153106. Epub 2009 May 22. PMID: 19470487;
718 PMCID: PMC2695064.

719 des Georges A, Dhote V, Kuhn L, Hellen CU, Pestova TV, Frank J, Hashem Y. Structure of
720 mammalian eIF3 in the context of the 43S preinitiation complex. Nature. 2015 Sep
721 24;525(7570):491-5. doi: 10.1038/nature14891. Epub 2015 Sep 7. PMID: 26344199; PMCID:
722 PMC4719162.

723 Dorn G, Gmeiner C, de Vries T, Dedic E, Novakovic M, Damberger FF, Maris C, Finol E, Sarnowski
724 CP, Kohlbrecher J, Welsh TJ, Bolisetty S, Mezzenga R, Aebersold R, Leitner A, Yulikov M, Jeschke
725 G, Allain FH. Integrative solution structure of PTBP1-IRES complex reveals strong compaction
726 and ordering with residual conformational flexibility. Nat Commun. 2023 Oct 13;14(1):6429.
727 doi: 10.1038/s41467-023-42012-z. PMID: 37833274; PMCID: PMC10576089.

728 Duke GM, Hoffman MA, Palmenberg AC. Sequence and structural elements that contribute to
729 efficient encephalomyocarditis virus RNA translation. J Virol. 1992 Mar;66(3):1602-9. doi:
730 10.1128/JVI.66.3.1602-1609.1992. PMID: 1310768; PMCID: PMC240893.

731 Eliseev B, Yeramala L, Leitner A, Karuppasamy M, Raimondeau E, Huard K, Alkalaeva E,
732 Aebersold R, Schaffitzel C. Structure of a human cap-dependent 48S translation pre-initiation
733 complex. Nucleic Acids Res. 2018 Mar 16;46(5):2678-2689. doi: 10.1093/nar/gky054. PMID:
734 29401259; PMCID: PMC5861459.

735 Emsley P, Lohkamp B, Scott WG, Cowtan K. Features and development of Coot. Acta Crystallogr
736 D Biol Crystallogr. 2010 Apr;66(Pt 4):486-501. doi: 10.1107/S0907444910007493. Epub 2010
737 Mar 24. PMID: 20383002; PMCID: PMC2852313.

738 Fernández IS, Bai XC, Murshudov G, Scheres SH, Ramakrishnan V. Initiation of translation by
739 cricket paralysis virus IRES requires its translocation in the ribosome. Cell. 2014 May
740 8;157(4):823-31. doi: 10.1016/j.cell.2014.04.015. Epub 2014 May 1. PMID: 24792965; PMCID:
741 PMC4017093.

742 Fernández N, Fernandez-Miragall O, Ramajo J, García-Sacristán A, Bellora N, Eyras E, Briones
743 C, Martínez-Salas E. Structural basis for the biological relevance of the invariant apical stem in
744 IRES-mediated translation. Nucleic Acids Res. 2011 Oct;39(19):8572-85. doi:
745 10.1093/nar/gkr560. Epub 2011 Jul 8. PMID: 21742761; PMCID: PMC3201876.

746 Fernández-Miragall O, López de Quinto S, Martínez-Salas E. Relevance of RNA structure for
747 the activity of picornavirus IRES elements. Virus Res. 2009 Feb;139(2):172-82. doi:
748 10.1016/j.virusres.2008.07.009. Epub 2008 Aug 15. PMID: 18692097.

749 Fernández-Miragall O, Martínez-Salas E. Structural organization of a viral IRES depends on the
750 integrity of the GNRA motif. RNA. 2003 Nov;9(11):1333-44. doi: 10.1261/rna.5950603. PMID:
751 14561883; PMCID: PMC1287055.

752 Fiore JL, Nesbitt DJ. An RNA folding motif: GNRA tetraloop-receptor interactions. Q Rev
753 Biophys. 2013 Aug;46(3):223-64. doi: 10.1017/S0033583513000048. Epub 2013 Aug 5. PMID:
754 23915736.

755 Gruber AR, Lorenz R, Bernhart SH, Neuböck R, Hofacker IL. The Vienna RNA websuite. Nucleic
756 Acids Res. 2008 Jul 1;36(Web Server issue):W70-4. doi: 10.1093/nar/gkn188. Epub 2008 Apr
757 19. PMID: 18424795; PMCID: PMC2447809.

758 Hashem Y, des Georges A, Dhote V, Langlois R, Liao HY, Grassucci RA, Pestova TV, Hellen CU,
759 Frank J. Hepatitis-C-virus-like internal ribosome entry sites displace eIF3 to gain access to the
760 40S subunit. Nature. 2013 Nov 28;503(7477):539-43. doi: 10.1038/nature12658. Epub 2013
761 Nov 3. PMID: 24185006; PMCID: PMC4106463.

762 Hashem Y, des Georges A, Dhote V, Langlois R, Liao HY, Grassucci RA, Hellen CU, Pestova TV,
763 Frank J. Structure of the mammalian ribosomal 43S preinitiation complex bound to the
764 scanning factor DHX29. Cell. 2013 May 23;153(5):1108-19. doi: 10.1016/j.cell.2013.04.036.
765 PMID: 23706745; PMCID: PMC3730827.

766 Hellen CU, Wimmer E. Translation of encephalomyocarditis virus RNA by internal ribosomal
767 entry. Curr Top Microbiol Immunol. 1995;203:31-63. doi: 10.1007/978-3-642-79663-0_2.
768 PMID: 7555090.

769 Hinnebusch AG. Structural Insights into the Mechanism of Scanning and Start Codon
770 Recognition in Eukaryotic Translation Initiation. Trends Biochem Sci. 2017 Aug;42(8):589-611.
771 doi: 10.1016/j.tibs.2017.03.004. Epub 2017 Apr 22. PMID: 28442192.

772 Hussain T, Llácer JL, Fernández IS, Munoz A, Martin-Marcos P, Savva CG, Lorsch JR, Hinnebusch
773 AG, Ramakrishnan V. Structural changes enable start codon recognition by the eukaryotic
774 translation initiation complex. Cell. 2014 Oct 23;159(3):597-607. doi:
775 10.1016/j.cell.2014.10.001. Epub 2014 Oct 16. PMID: 25417110; PMCID: PMC4217140.

776 Imai S, Kumar P, Hellen CU, D'Souza VM, Wagner G. An accurately preorganized IRES RNA
777 structure enables eIF4G capture for initiation of viral translation. Nat Struct Mol Biol. 2016
778 Sep;23(9):859-64. doi: 10.1038/nsmb.3280. Epub 2016 Aug 15. PMID: 27525590; PMCID:
779 PMC5061125.

780 Imai S, Suzuki H, Fujiyoshi Y, Shimada I. Dynamically regulated two-site interaction of viral RNA
781 to capture host translation initiation factor. Nat Commun. 2023 Aug 28;14(1):4977. doi:
782 10.1038/s41467-023-40582-6. PMID: 37640715; PMCID: PMC10462655.

783 International Committee on Taxonomy of Viruses Executive Committee. The new scope of
784 virus taxonomy: partitioning the virosphere into 15 hierarchical ranks. Nat Microbiol. 2020
785 May;5(5):668-674. doi: 10.1038/s41564-020-0709-x. Epub 2020 Apr 27. PMID: 32341570;
786 PMCID: PMC7186216.

787 Jackson RJ, Hellen CU, Pestova TV. The mechanism of eukaryotic translation initiation and
788 principles of its regulation. Nat Rev Mol Cell Biol. 2010 Feb;11(2):113-27. doi:
789 10.1038/nrm2838. PMID: 20094052; PMCID: PMC4461372.

790 Jang SK, Kräusslich HG, Nicklin MJ, Duke GM, Palmenberg AC, Wimmer E. A segment of the 5'
791 nontranslated region of encephalomyocarditis virus RNA directs internal entry of ribosomes
792 during in vitro translation. J Virol. 1988 Aug;62(8):2636-43. doi: 10.1128/JVI.62.8.2636-
793 2643.1988. PMID: 2839690; PMCID: PMC253694.

794 Johnson AG, Grosely R, Petrov AN, Puglisi JD. Dynamics of IRES-mediated translation. Philos
795 Trans R Soc Lond B Biol Sci. 2017 Mar 19;372(1716):20160177. doi: 10.1098/rstb.2016.0177.
796 PMID: 28138065; PMCID: PMC5311923.

797 Kafasla P, Morgner N, Pöyry TA, Curry S, Robinson CV, Jackson RJ. Polypyrimidine tract binding
798 protein stabilizes the encephalomyocarditis virus IRES structure via binding multiple sites in a
799 unique orientation. Mol Cell. 2009 Jun 12;34(5):556-68. doi: 10.1016/j.molcel.2009.04.015.
800 PMID: 19524536.

801 Kafasla P, Morgner N, Robinson CV, Jackson RJ. Polypyrimidine tract-binding protein stimulates
802 the poliovirus IRES by modulating eIF4G binding. EMBO J. 2010 Nov 3;29(21):3710-22. doi:
803 10.1038/emboj.2010.231. Epub 2010 Sep 21. PMID: 20859255; PMCID: PMC2982756.

804 Kaminski A, Belsham GJ, Jackson RJ. Translation of encephalomyocarditis virus RNA:
805 parameters influencing the selection of the internal initiation site. EMBO J. 1994 Apr
806 1;13(7):1673-81. doi: 10.1002/j.1460-2075.1994.tb06431.x. PMID: 8157006; PMCID:
807 PMC394998.

808 Khatter H, Myasnikov AG, Natchiar SK, Klaholz BP. Structure of the human 80S ribosome.
809 Nature. 2015 Apr 30;520(7549):640-5. doi: 10.1038/nature14427. Epub 2015 Apr 22. PMID:
810 25901680.

811 Kim H, Kim K, Kwon T, Kim DW, Kim SS, Kim YJ. Secondary structure conservation of the stem-
812 loop IV sub-domain of internal ribosomal entry sites in human rhinovirus clinical isolates. Int
813 J Infect Dis. 2015 Dec;41:21-8. doi: 10.1016/j.ijid.2015.10.015. Epub 2015 Oct 27. PMID:
814 26518063.

815 Kolupaeva VG, Pestova TV, Hellen CU, Shatsky IN. Translation eukaryotic initiation factor 4G
816 recognizes a specific structural element within the internal ribosome entry site of
817 encephalomyocarditis virus RNA. J Biol Chem. 1998 Jul 17;273(29):18599-604. doi:
818 10.1074/jbc.273.29.18599. PMID: 9660832.

819 Kozak M. The scanning model for translation: an update. J Cell Biol. 1989 Feb;108(2):229-41.
820 doi: 10.1083/jcb.108.2.229. PMID: 2645293; PMCID: PMC2115416.

821 Kwon OS, An S, Kim E, Yu J, Hong KY, Lee JS, Jang SK. An mRNA-specific tRNAi carrier eIF2A
822 plays a pivotal role in cell proliferation under stress conditions: stress-resistant translation of
823 c-Src mRNA is mediated by eIF2A. Nucleic Acids Res. 2017 Jan 9;45(1):296-310. doi:
824 10.1093/nar/gkw1117. Epub 2016 Nov 28. PMID: 27899592; PMCID: PMC5224483.

825 Lee KM, Chen CJ, Shih SR. Regulation Mechanisms of Viral IRES-Driven Translation. Trends
826 Microbiol. 2017 Jul;25(7):546-561. doi: 10.1016/j.tim.2017.01.010. Epub 2017 Feb 24. PMID:
827 28242053.

828 Liang Z, Kumar AS, Jones MS, Knowles NJ, Lipton HL. Phylogenetic analysis of the species
829 Theilovirus: emerging murine and human pathogens. J Virol. 2008 Dec;82(23):11545-54. doi:
830 10.1128/JVI.01160-08. Epub 2008 Sep 24. PMID: 18815294; PMCID: PMC2583687.

831 Liebschner D, Afonine PV, Baker ML, Bunkóczi G, Chen VB, Croll TI, Hintze B, Hung LW, Jain S,
832 McCoy AJ, Moriarty NW, Oeffner RD, Poon BK, Prisant MG, Read RJ, Richardson JS, Richardson
833 DC, Sammito MD, Sobolev OV, Stockwell DH, Terwilliger TC, Urzhumtsev AG, Videau LL,
834 Williams CJ, Adams PD. Macromolecular structure determination using X-rays, neutrons and
835 electrons: recent developments in Phenix. Acta Crystallogr D Struct Biol. 2019 Oct 1;75(Pt
836 10):861-877. doi: 10.1107/S2059798319011471. Epub 2019 Oct 2. PMID: 31588918; PMCID:
837 PMC6778852.

838 Llácer JL, Hussain T, Marler L, Aitken CE, Thakur A, Lorsch JR, Hinnebusch AG, Ramakrishnan
839 V. Conformational Differences between Open and Closed States of the Eukaryotic Translation
840 Initiation Complex. Mol Cell. 2015 Aug 6;59(3):399-412. doi: 10.1016/j.molcel.2015.06.033.
841 Epub 2015 Jul 23. PMID: 26212456; PMCID: PMC4534855.

842 Llácer JL, Hussain T, Dong J, Villamayor L, Gordiyenko Y, Hinnebusch AG. Large-scale movement
843 of eIF3 domains during translation initiation modulate start codon selection. Nucleic Acids
844 Res. 2021 Nov 18;49(20):11491-11511. doi: 10.1093/nar/gkab908. PMID: 34648019; PMCID:
845 PMC8599844.

846 Lomakin IB, Hellen CU, Pestova TV. Physical association of eukaryotic initiation factor 4G
847 (eIF4G) with eIF4A strongly enhances binding of eIF4G to the internal ribosomal entry site of
848 encephalomyocarditis virus and is required for internal initiation of translation. Mol Cell Biol.
849 2000 Aug;20(16):6019-29. doi: 10.1128/mcb.20.16.6019-6029.2000. PMID: 10913184;
850 PMCID: PMC86078.

851 López de Quinto S, Martínez-Salas E. Conserved structural motifs located in distal loops of
852 aphthovirus internal ribosome entry site domain 3 are required for internal initiation of
853 translation. J Virol. 1997 May;71(5):4171-5. doi: 10.1128/JVI.71.5.4171-4175.1997. PMID:
854 9094703; PMCID: PMC191578.

855 Lozano G, Martínez-Salas E. Structural insights into viral IRES-dependent translation
856 mechanisms. Curr Opin Virol. 2015 Jun;12:113-20. doi: 10.1016/j.coviro.2015.04.008. Epub
857 2015 May 22. PMID: 26004307.

858 Lozano G, Francisco-Velilla R, Martinez-Salas E. Ribosome-dependent conformational
859 flexibility changes and RNA dynamics of IRES domains revealed by differential SHAPE. Sci Rep.
860 2018 Apr 3;8(1):5545. doi: 10.1038/s41598-018-23845-x. PMID: 29615727; PMCID:
861 PMC5882922.

862 Maloney A, Joseph S. Validating the EMCV IRES Secondary Structure with Structure-Function
863 Analysis. Biochemistry. 2024 Jan 2;63(1):107-115. doi: 10.1021/acs.biochem.3c00579. Epub
864 2023 Dec 11. PMID: 38081770; PMCID: PMC10896073.

865 Maris C, Jayne S, Damberger FF, Beusch I, Dorn G, Ravindranathan S, Allain FH. A transient α-
866 helix in the N-terminal RNA recognition motif of polypyrimidine tract binding protein senses
867 RNA secondary structure. Nucleic Acids Res. 2020 May 7;48(8):4521-4537. doi:
868 10.1093/nar/gkaa155. PMID: 32170319; PMCID: PMC7192611.

869 Martinez-Salas E, Francisco-Velilla R, Fernandez-Chamorro J, Embarek AM. Insights into
870 Structural and Mechanistic Features of Viral IRES Elements. Front Microbiol. 2018 Jan
871 4;8:2629. doi: 10.3389/fmicb.2017.02629. PMID: 29354113; PMCID: PMC5759354.

872 Martínez-Salas E, Francisco-Velilla R, Fernandez-Chamorro J, Lozano G, Diaz-Toledano R.
873 Picornavirus IRES elements: RNA structure and host protein interactions. Virus Res. 2015 Aug
874 3;206:62-73. doi: 10.1016/j.virusres.2015.01.012. Epub 2015 Jan 21. PMID: 25617758

875 Muhs M, Hilal T, Mielke T, Skabkin MA, Sanbonmatsu KY, Pestova TV, Spahn CM. Cryo-EM of
876 ribosomal 80S complexes with termination factors reveals the translocated cricket paralysis
877 virus IRES. Mol Cell. 2015 Feb 5;57(3):422-32. doi: 10.1016/j.molcel.2014.12.016. Epub 2015
878 Jan 15. PMID: 25601755; PMCID: PMC4526138.

879 Murray J, Savva CG, Shin BS, Dever TE, Ramakrishnan V, Fernández IS. Structural
880 characterization of ribosome recruitment and translocation by type IV IRES. Elife. 2016 May
881 9;5:e13567. doi: 10.7554/eLife.13567. PMID: 27159451; PMCID: PMC4861600.

882 Neupane R, Pisareva VP, Rodriguez CF, Pisarev AV, Fernández IS. A complex IRES at the 5'-UTR
883 of a viral mRNA assembles a functional 48S complex via an uAUG intermediate. Elife. 2020 Apr
884 14;9:e54575. doi: 10.7554/eLife.54575. PMID: 32286223; PMCID: PMC7190351.

885 Niepmann M, Gerresheim GK. Hepatitis C Virus Translation Regulation. Int J Mol Sci. 2020 Mar
886 27;21(7):2328. doi: 10.3390/ijms21072328. PMID: 32230899; PMCID: PMC7178104.

887 Ochs K, Saleh L, Bassili G, Sonntag VH, Zeller A, Niepmann M. Interaction of translation
888 initiation factor eIF4B with the poliovirus internal ribosome entry site. J Virol. 2002
889 Mar;76(5):2113-22. doi: 10.1128/jvi.76.5.2113-2122.2002. PMID: 11836388; PMCID:
890 PMC135939.

891 Pelletier J, Sonenberg N. Internal initiation of translation of eukaryotic mRNA directed by a
892 sequence derived from poliovirus RNA. Nature. 1988 Jul 28;334(6180):320-5. doi:
893 10.1038/334320a0. PMID: 2839775.

894 Pestova TV, Hellen CU, Shatsky IN. Canonical eukaryotic initiation factors determine initiation
895 of translation by internal ribosomal entry. Mol Cell Biol. 1996 Dec;16(12):6859-69. doi:
896 10.1128/MCB.16.12.6859. PMID: 8943341; PMCID: PMC231689.

897 Petrov A, Grosely R, Chen J, O'Leary SE, Puglisi JD. Multiple Parallel Pathways of Translation
898 Initiation on the CrPV IRES. Mol Cell. 2016 Apr 7;62(1):92-103. doi:
899 10.1016/j.molcel.2016.03.020. PMID: 27058789; PMCID: PMC4826567.

900 Petrychenko V, Yi SH, Liedtke D, Peng BZ, Rodnina MV, Fischer N. Structural basis for
901 translational control by the human 48S initiation complex. Nat Struct Mol Biol. 2024 Sep 17.
902 doi: 10.1038/s41594-024-01378-4. Epub ahead of print. PMID: 39289545.

903 Pettersen EF, Goddard TD, Huang CC, Couch GS, Greenblatt DM, Meng EC, Ferrin TE. UCSF
904 Chimera--a visualization system for exploratory research and analysis. J Comput Chem. 2004
905 Oct;25(13):1605-12. doi: 10.1002/jcc.20084. PMID: 15264254.

906 Pettersen EF, Goddard TD, Huang CC, Meng EC, Couch GS, Croll TI, Morris JH, Ferrin TE. UCSF
907 ChimeraX: Structure visualization for researchers, educators, and developers. Protein Sci.
908 2021 Jan;30(1):70-82. doi: 10.1002/pro.3943. Epub 2020 Oct 22. PMID: 32881101; PMCID:
909 PMC7737788.

910 Punjani A, Rubinstein JL, Fleet DJ, Brubaker MA. cryoSPARC: algorithms for rapid unsupervised
911 cryo-EM structure determination. Nat Methods. 2017 Mar;14(3):290-296. doi:
912 10.1038/nmeth.4169. Epub 2017 Feb 6. PMID: 28165473.

913 Punjani A, Zhang H, Fleet DJ. Non-uniform refinement: adaptive regularization improves
914 single-particle cryo-EM reconstruction. Nat Methods. 2020 Dec;17(12):1214-1221. doi:
915 10.1038/s41592-020-00990-8. Epub 2020 Nov 30. PMID: 33257830.

916 Quade N, Boehringer D, Leibundgut M, van den Heuvel J, Ban N. Cryo-EM structure of
917 Hepatitis C virus IRES bound to the human ribosome at 3.9-Å resolution. Nat Commun. 2015
918 Jul 8;6:7646. doi: 10.1038/ncomms8646. PMID: 26155016; PMCID: PMC4510694.

919 Reiter NJ, Osterman A, Torres-Larios A, Swinger KK, Pan T, Mondragón A. Structure of a
920 bacterial ribonuclease P holoenzyme in complex with tRNA. Nature. 2010 Dec
921 9;468(7325):784-9. doi: 10.1038/nature09516. Epub 2010 Nov 14. PMID: 21076397; PMCID:
922 PMC3058908.

923 Roberts LO, Belsham GJ. Complementation of defective picornavirus internal ribosome entry
924 site (IRES) elements by the coexpression of fragments of the IRES. Virology. 1997 Jan
925 6;227(1):53-62. doi: 10.1006/viro.1996.8312. PMID: 9007058.

926 Robertson ME, Seamons RA, Belsham GJ. A selection system for functional internal ribosome
927 entry site (IRES) elements: analysis of the requirement for a conserved GNRA tetraloop in the
928 encephalomyocarditis virus IRES. RNA. 1999 Sep;5(9):1167-79. doi:
929 10.1017/s1355838299990301. PMID: 10496218; PMCID: PMC1369840.

930 Scheper GC, Thomas AA, Voorma HO. The 5' untranslated region of encephalomyocarditis
931 virus contains a sequence for very efficient binding of eukaryotic initiation factor eIF-2/2B.
932 Biochim Biophys Acta. 1991 Jun 13;1089(2):220-6. doi: 10.1016/0167-4781(91)90011-a.
933 PMID: 1647211.

934 Scheper GC, Voorma HO, Thomas AA. Binding of eukaryotic initiation factor-2 and trans-acting
935 factors to the 5' untranslated region of encephalomyocarditis virus RNA. Biochimie.
936 1994;76(8):801-9. doi: 10.1016/0300-9084(94)90084-1. PMID: 7893829.

Sievers F, Higgins DG. The Clustal Omega Multiple Alignment Package. Methods Mol Biol. 2021;2231:3-16. doi: 10.1007/978-1-0716-1036-7_1. PMID: 33289883.

Simonetti A, Guca E, Bochler A, Kuhn L, Hashem Y. Structural Insights into the Mammalian Late-Stage Initiation Complexes. Cell Rep. 2020 Apr 7;31(1):107497. doi: 10.1016/j.celrep.2020.03.061. PMID: 32268096; PMCID: PMC7166083.

Spahn CM, Jan E, Mulder A, Grassucci RA, Sarnow P, Frank J. Cryo-EM visualization of a viral internal ribosome entry site bound to human ribosomes: the IRES functions as an RNA-based translation factor. Cell. 2004 Aug 20;118(4):465-75. doi: 10.1016/j.cell.2004.08.001. PMID: 15315759.

Spahn CM, Kieft JS, Grassucci RA, Penczek PA, Zhou K, Doudna JA, Frank J. Hepatitis C virus IRES RNA-induced changes in the conformation of the 40s ribosomal subunit. Science. 2001 Mar 9;291(5510):1959-62. doi: 10.1126/science.1058409. PMID: 11239155.

Sweeney TR, Abaeva IS, Pestova TV, Hellen CU. The mechanism of translation initiation on Type 1 picornavirus IRESs. EMBO J. 2014 Jan 7;33(1):76-92. doi: 10.1002/embj.201386124. Epub 2013 Dec 15. PMID: 24357634; PMCID: PMC3990684.

Trono D, Pelletier J, Sonenberg N, Baltimore D. Translation in mammalian cells of a gene linked to the poliovirus 5' noncoding region. Science. 1988 Jul 22;241(4864):445-8. doi: 10.1126/science.2839901. PMID: 2839901.

Velazquez MA, Nuthalapati SS, Hankinson J, Fominykh K, Lulla V, Sweeney TR, Hill CH. Structural and mechanistic insights into translation initiation on the enterovirus Type 1 IRES. bioRxiv [Preprint]. 2025 Oct 3: 2025.10.04.680434. doi: 10.1101/2025.10.04.680434.

Villa N, Do A, Hershey JW, Fraser CS. Human eukaryotic initiation factor 4G (eIF4G) protein binds to eIF3c, -d, and -e to promote mRNA recruitment to the ribosome. J Biol Chem. 2013 Nov 15;288(46):32932-40. doi: 10.1074/jbc.M113.517011. Epub 2013 Oct 3. PMID: 24092755; PMCID: PMC3829144.

Villamayor-Belinchón L, Sharma P, Gordiyenko Y, Llácer JL, Hussain T. Structural basis of AUC codon discrimination during translation initiation in yeast. Nucleic Acids Res. 2024 Oct 14;52(18):11317-11335. doi: 10.1093/nar/gkae737. PMID: 39193907; PMCID: PMC11472065.

Welnowska E, Sanz MA, Redondo N, Carrasco L. Translation of viral mRNA without active eIF2: the case of picornaviruses. PLoS One. 2011;6(7):e22230. doi: 10.1371/journal.pone.0022230. Epub 2011 Jul 14. PMID: 21779397; PMCID: PMC3136507.

Yamamoto H, Collier M, Loerke J, Ismer J, Schmidt A, Hilal T, Sprink T, Yamamoto K, Mielke T, Bürger J, Shaikh TR, Dabrowski M, Hildebrand PW, Scheerer P, Spahn CM. Molecular architecture of the ribosome-bound Hepatitis C Virus internal ribosomal entry site RNA. EMBO J. 2015 Dec 14;34(24):3042-58. doi: 10.15252/embj.201592469. Epub 2015 Nov 24. PMID: 26604301; PMCID: PMC4687786.

Yamamoto H, Unbehaun A, Loerke J, Behrmann E, Collier M, Bürger J, Mielke T, Spahn CM. Structure of the mammalian 80S initiation complex with initiation factor 5B on HCV-IRES RNA.

975 Nat Struct Mol Biol. 2014 Aug;21(8):721-7. doi: 10.1038/nsmb.2859. Epub 2014 Jul 27. PMID:
976 25064512.

977 Yi SH, Petrychenko V, Schliep JE, Goyal A, Linden A, Chari A, Urlaub H, Stark H, Rodnina MV,
978 Adio S, Fischer N. Conformational rearrangements upon start codon recognition in human 48S
979 translation initiation complex. Nucleic Acids Res. 2022 May 20;50(9):5282-5298. doi:
980 10.1093/nar/gkac283. PMID: 35489072; PMCID: PMC9122606.

981 Yokoyama T, Machida K, Iwasaki W, Shigeta T, Nishimoto M, Takahashi M, Sakamoto A,
982 Yonemochi M, Harada Y, Shigematsu H, Shirouzu M, Tadakuma H, Imataka H, Ito T. HCV IRES
983 Captures an Actively Translating 80S Ribosome. Mol Cell. 2019 Jun 20;74(6):1205-1214.e8.
984 doi: 10.1016/j.molcel.2019.04.022. Epub 2019 May 9. PMID: 31080011.

985 Yu Y, Abaeva IS, Marintchev A, Pestova TV, Hellen CU. Common conformational changes
986 induced in type 2 picornavirus IRESs by cognate trans-acting factors. Nucleic Acids Res. 2011
987 Jun;39(11):4851-65. doi: 10.1093/nar/gkr045. Epub 2011 Feb 8. PMID: 21306989; PMCID:
988 PMC3113573.

989 Zhao J, Li Y, Wang C, Zhang H, Zhang H, Jiang B, Guo X, Song X. IRESbase: A Comprehensive
990 Database of Experimentally Validated Internal Ribosome Entry Sites. Genomics Proteomics
991 Bioinformatics. 2020 Apr;18(2):129-139. doi: 10.1016/j.gpb.2020.03.001. Epub 2020 Jun 6.
992 PMID: 32512182; PMCID: PMC7646085.

A

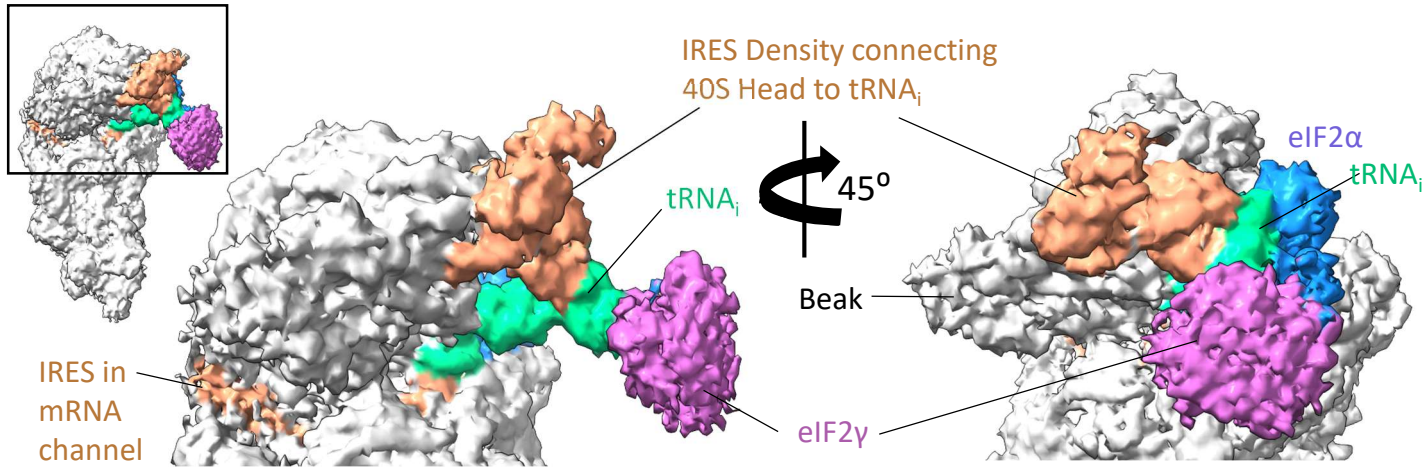
IRES Density connecting
40S Head to tRNA$_i$
tRNA$_i$
45°
eIF2α
tRNA$_i$
Beak
IRES in
mRNA
channel
eIF2γ

B

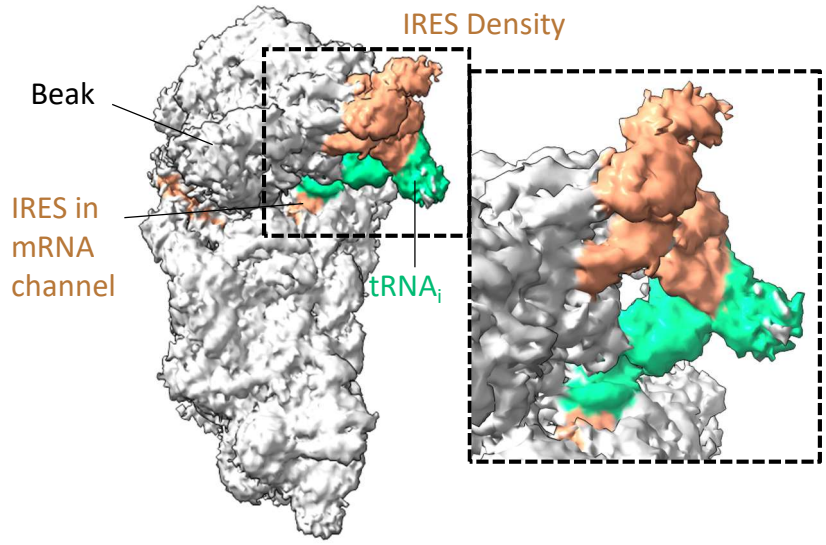
IRES Density
Beak
IRES in
mRNA
channel
tRNA$_i$

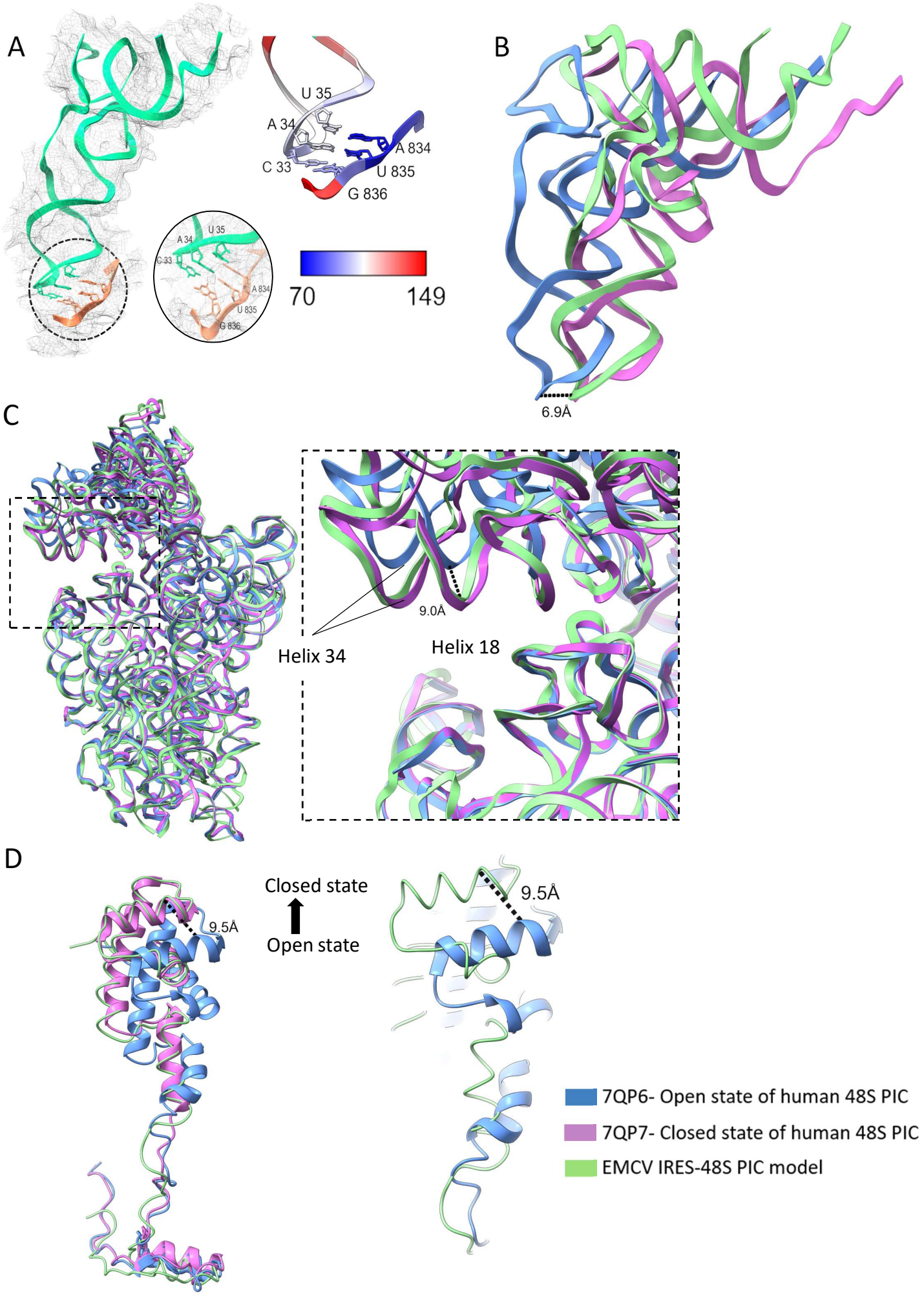
A
U 35
A 34
C 33
A 834
U 835
G 836
70
149
B
6.9Å
C
9.0Å
Helix 34
Helix 18
D
9.5Å
Closed state
Open state
9.5Å
7QP6- Open state of human 48S PIC
7QP7- Closed state of human 48S PIC
EMCV IRES-48S PIC model

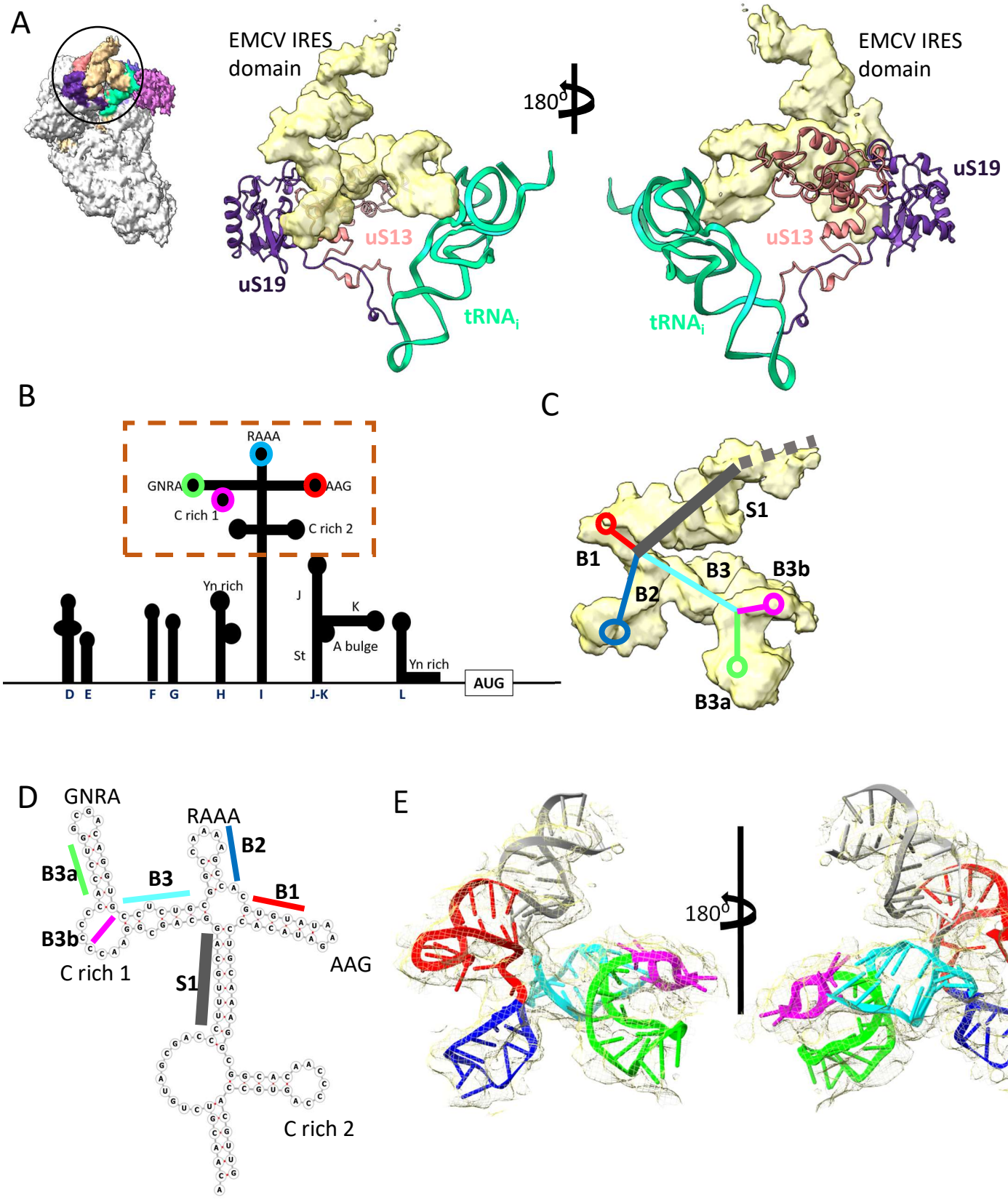
A
EMCV IRES domain
uS13
uS19
tRNA$_i$
180°
EMCV IRES domain
uS19
uS13
tRNA$_i$
B
RAAA
GNRA
AAG
C rich 1
C rich 2
Yn rich
J
K
St
A bulge
Yn rich
AUG
D E
F G
H
I
J-K
L
C
S1
B1
B3
B3b
B2
B3a
D
GNRA
RAAA
B2
B3a
B3
B1
B3b
C rich 1
AAG
S1
C rich 2
E
180°

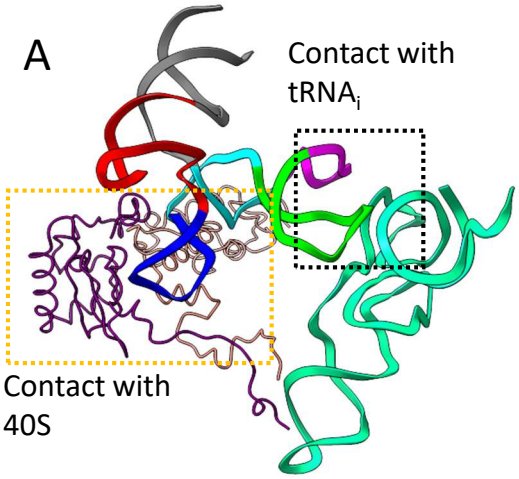
A
Contact with
tRNA$_i$
Contact with
40S

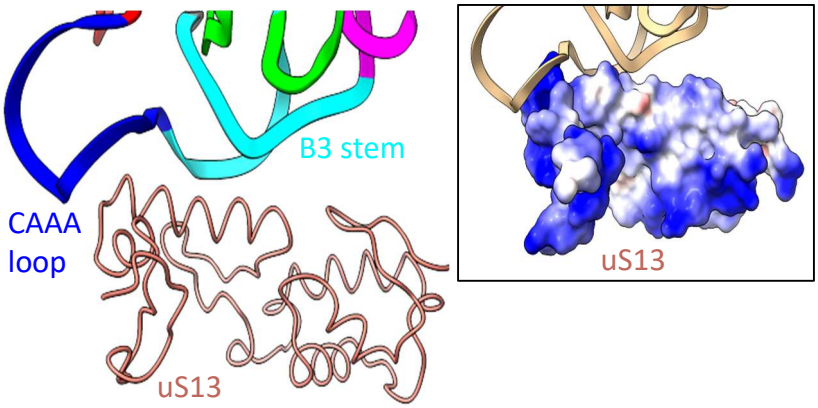
B
B3 stem
CAAA
loop
uS13
uS13

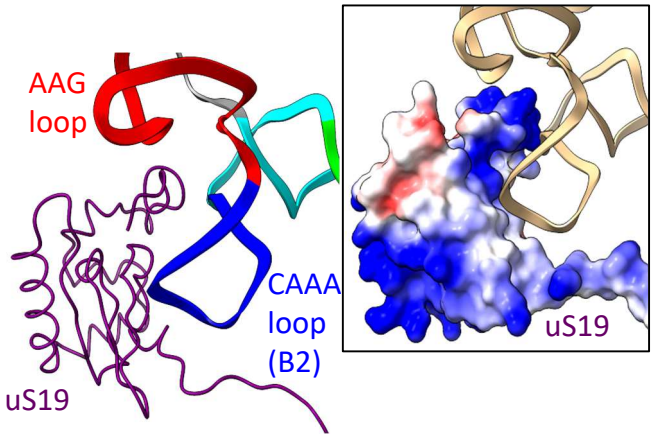
C
AAG
loop
CAAA
loop
(B2)
uS19
uS19

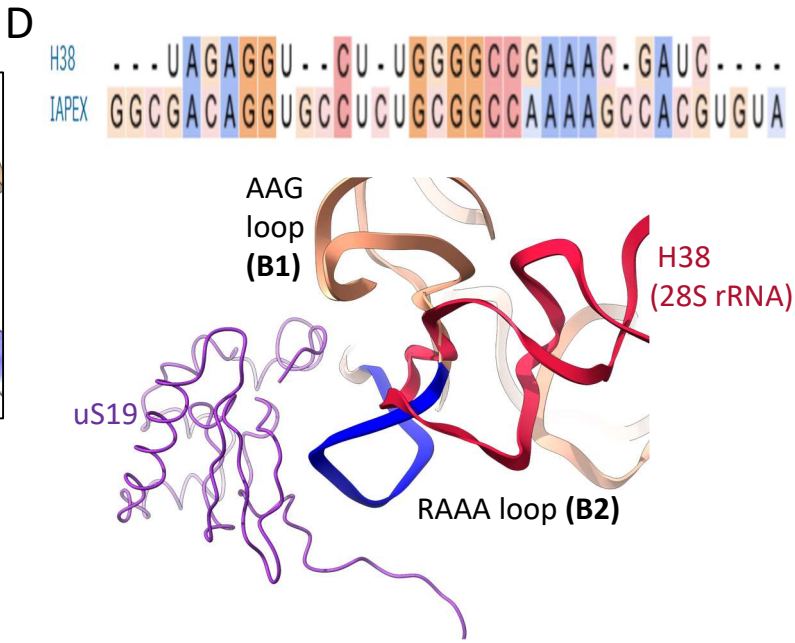
D
H38 ...UAGAGGU..CU.UGGGGCCGAAAC.GAUC....
IAPEX GGCGACAGGUGCCUCUGCGGCCAAAAGCCACGUGUA
AAG
loop
(B1)
H38
(28S rRNA)
uS19
RAAA loop (B2)

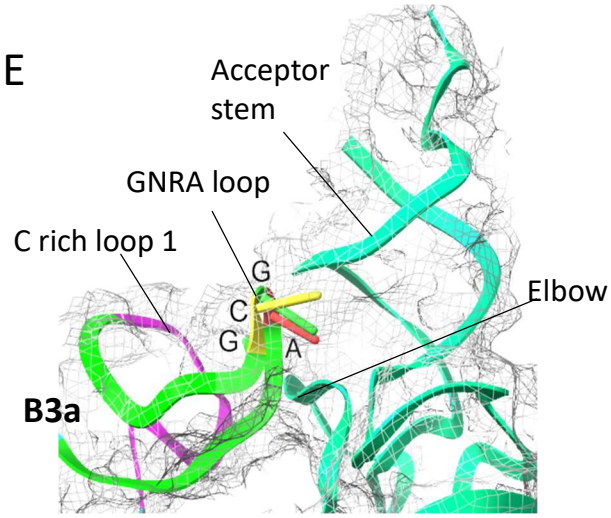
E
Acceptor
stem
GNRA loop
C rich loop 1
G
C
G
A
Elbow
B3a

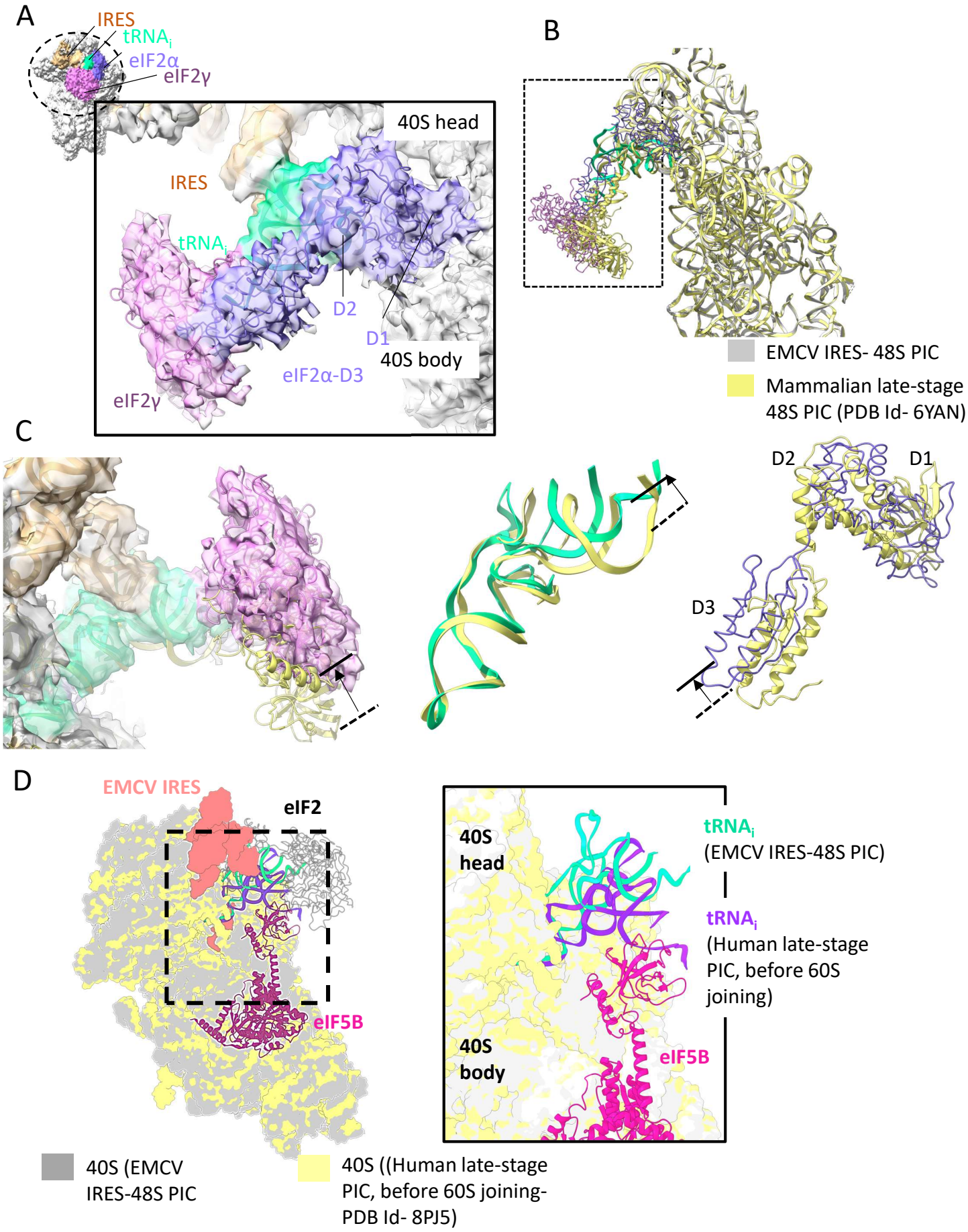
A
IRES
tRNA$_i$
eIF2α
eIF2γ
40S head
IRES
tRNA$_i$
D2
D1
40S body
eIF2α-D3
eIF2γ
B
EMCV IRES- 48S PIC
Mammalian late-stage 48S PIC (PDB Id- 6YAN)
C
D2
D1
D3
D
EMCV IRES
eIF2
eIF5B
40S head
tRNA$_i$ (EMCV IRES-48S PIC)
tRNA$_i$ (Human late-stage PIC, before 60S joining)
40S body
eIF5B
40S (EMCV IRES-48S PIC
40S ((Human late-stage PIC, before 60S joining- PDB Id- 8PJ5)

A

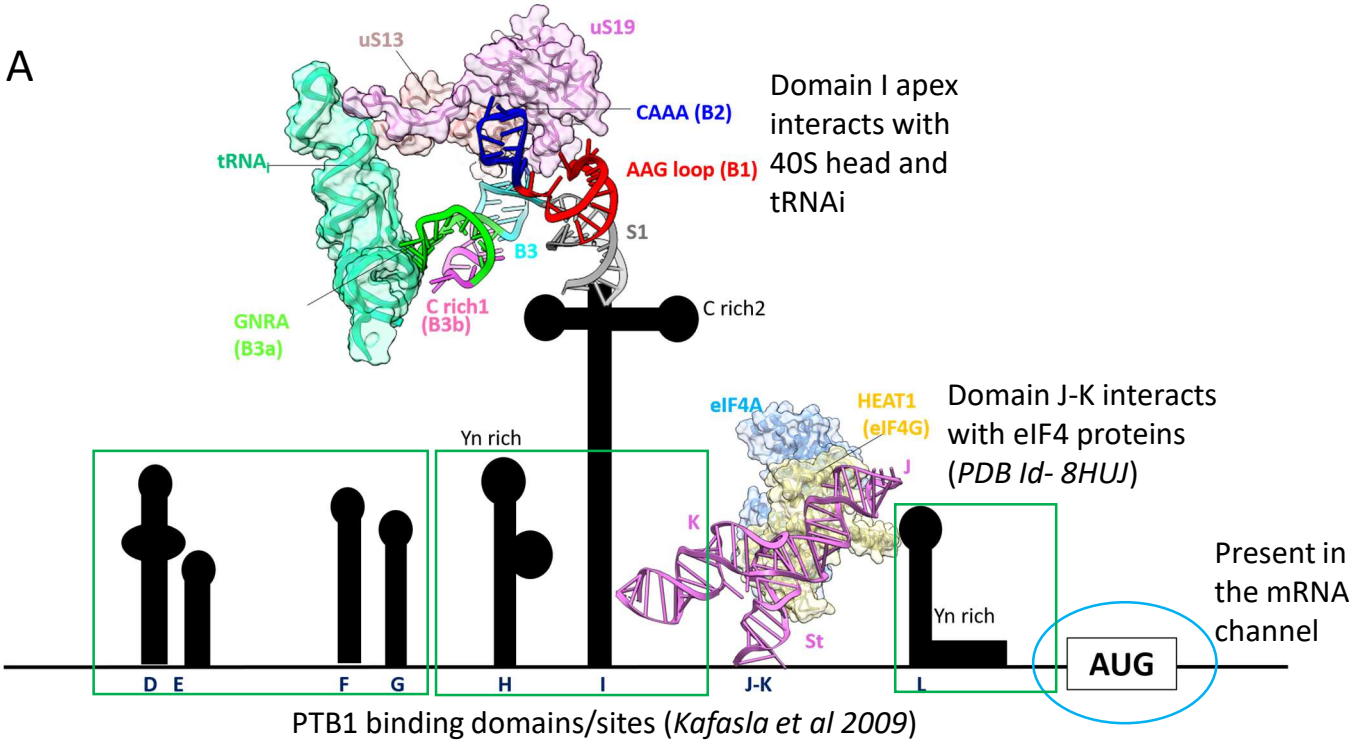

PTB1 binding domains/sites (*Kafasla et al 2009*)

B

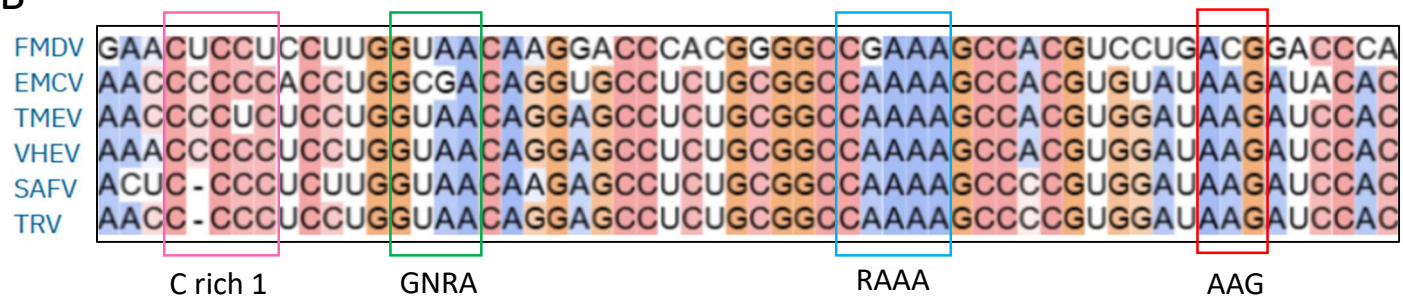
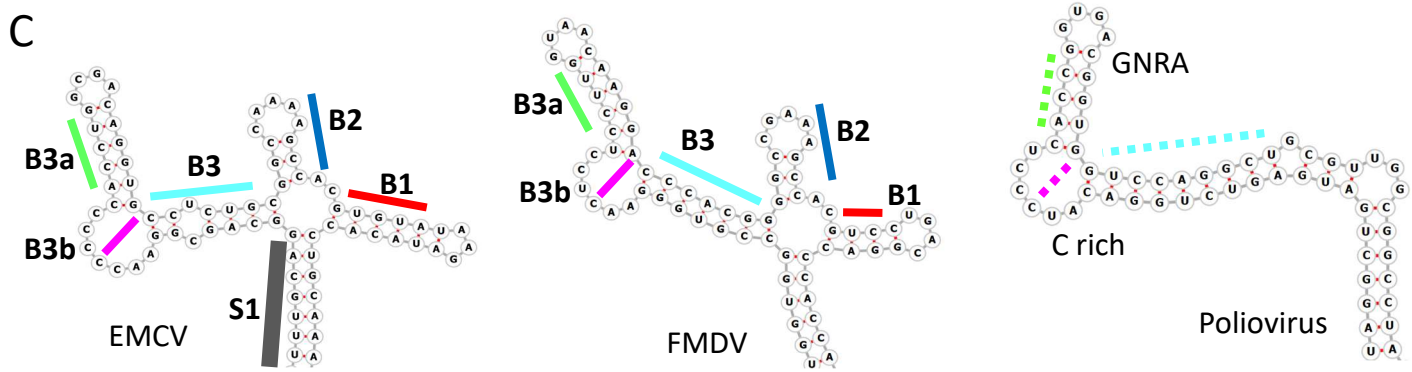
C